MICS-Asia III: Multi-model comparison of reactive Nitrogen deposition over China

Baozhu Ge[1,2], Syuichi Itahashi[3], Keiichi Sato[4], Danhui Xu[1,5], Junhua Wang[1,5], Fan fan[6], Qixin Tan[1,5], Joshua S. Fu[7], Xuemei Wang[8], Kazuyo Yamaji[9], Tatsuya Nagashima[10], Jie Li[1,2,5], Mizuo Kajino[11,12], Hong Liao[13], Meigen Zhang[1,2,5], Zhe Wang[1,2,14], Meng Li[15], Jung-Hun Woo[16], Jun-ichi Kurokawa[17], Yuepen Pan[1], Qizhong Wu[18], Xuejun Liu[19] and Zifa Wang[1,2,5]

[1] State Key Laboratory of Atmospheric Boundary Layer Physics and Atmospheric Chemistry (LAPC), Institute of Atmospheric Physics (IAP), Chinese Academy of Sciences (CAS), Beijing 100029, China

[2] Center for Excellence in Urban Atmospheric Environment, Institute of Urban Environment, Chinese Academy of Sciences (CAS), Xiamen 361021, China

[3] Environmental Science Research Laboratory, Central Research Institute of Electric Power Industry (CRIEPI), Abiko, Chiba 270–1194, Japan

[4] Asia Center for Air Pollution Research (ACAP), 1182 Sowa, Nishi-ku, Niigata, Niigata 950-2144, Japan

[5] Collage of Earth Science, University of Chinese Academy of Sciences, Beijing 100049, China

[6] Nanjing Intelligent Environmental Sci-Tech Co., Ltd., Nanjing, 211800, China

[7] Department of Civil and Environmental Engineering, University of Tennessee, Knoxville, TN 37996, USA

[8] Institute for Environmental and Climate Research, Jinan University, Guangzhou 510632, China

[9] Graduate School of Maritime Sciences, Kobe University, Kobe, Hyogo 658–0022, Japan

[10] National Institute for Environmental Studies (NIES), Tsukuba, Ibaraki 305–8506, Japan

[11] Meteorological Research Institute (MRI), Tsukuba, Ibaraki 305–8506, Japan

[12] Faculty of Life and Environmental Sciences, University of Tsukuba, Tsukuba, Ibaraki 305–8506, Japan

[13] School of Environmental Science and Engineering, Nanjing University of Information Science & Technology, Nanjing 210044, China

[14] Research Institute for Applied Mechanics (RIAM), Kyushu Univeristy, Kasuga, Fukuoka 816–8580, Japan

[15] Ministry of Education Key Laboratory for Earth System Modeling, Department of Earth System Science, Tsinghua University, Beijing 100084, China

[16] Division of Interdisciplinary Studies, Department of Advance Technology Fusion, Konkuk University, Seoul, 303-804, Korea

[17] Asia Center for Air Pollution Research (ACAP), 1182 Sowa, Nishi-ku, Niigata, Niigata 950-2144, Japan

[18] College of Global Change and Earth System Science, Beijing Normal University, Beijing 100875, China

[19] College of Resources & Environmental Sciences, China Agricultural University, Beijing 100193, China.

Correspondence to: Baozhu Ge (gebz@mail.iap.ac.cn)

Abstract: Atmospheric nitrogen deposition in China has attracted public attention in recent years due to the increasing anthropogenic emission of reactive nitrogen (N_r) and its impacts on the terrestrial and aquatic ecosystems. However, limited long-term and multi-site measurements have restrained the understanding on the mechanism of the N_r deposition as well as the chemical transport model (CTM) improvement. In this study, the performance of the simulated wet and dry deposition for different N_r species, i.e., particulate NO_3^- and NH_4^+, gaseous NO_x, HNO_3 and NH_3, have been conducted using the framework of Model Inter-Comparison Study for Asia (MICS-Asia) phase III. Nine Models, including 5 WRF-CMAQ models, 2 self-developed regional models, a global model and a RAMS-CMAQ model, have been selected for the comparison. For wet depositions, observation data from 83 measurement sites of EANET, CREN, CAUDN, NADMN and DEE of China have been collected and normalized to compare with model results. In general, most models show the consistent spatial and temporal variation of both oxidized N (N_{ox}) and reduced N (N_{rd}) wet depositions in China with the NME around at 50%, which is lower than the value of 70% based on EANET observation over Asia. Both the ratio of wet or dry deposition to the total inorganic N deposition (TIN) and the ratios of TIN to their emissions have shown consistent results with the NNDMN estimates. The performance of ensemble results (ENM) was further assessed with satellite measurements. In different regions of China, the results show that the simulated N_{ox} wet deposition was overestimated in North East China (NE) but underestimated in south of China (SE+SW), while the N_{rd} wet deposition was underestimated in all regions by all models. The deposition of N_{ox} has larger uncertainties than the N_{rd} especially in North China (NC), indicating the chemical reaction process is one of the most important factors affecting the model performance. Compared to Critical Load (CL) value, the N_r deposition in NC, SE and SW reached or exceeded reported CL values and resulted in serious ecological impacts. The control of N_{rd} in NC and SW and N_{ox} in SE would be effective mitigations for TIN deposition in these regions. The N_r deposition in the Tibet plateau with a high ratio of TIN/emission (~3.0), indicates a significant transmission from outside. Efforts to reduce these transmissions ought to be a paramount goal, due the climatic importance of the Tibet region to sensitive ecosystems throughout China.

Keywords: Nitrogen deposition, multi-model comparison, China, reduced nitrogen, oxidized nitrogen

1 Introduction

Atmospheric Nitrogen (N) deposition is defined as N related gases and particles are deposited via precipitation (wet deposition) and not via precipitation (dry deposition) (Clark and Kremer, 2005). These deposits to the Earth's surface are either close to the sources or in remote regions (e.g. chemical transformation and long-range transport of oxidized and reduced N, N_{ox} and N_{rd} hereafter), located far from human activities and labeled as the N-limited areas (Phoenix et al., 2006;Holtgrieve et al., 2011). Evidence shows that the effects of reactive N (N_r=N_{ox}+N_{rd}) deposition to the environment are numerous, including decreased biological diversity, increased soil acidification, and lake eutrophication (Clark and Tilman, 2008;Janssens et al., 2010;Holtgrieve et al., 2011;Phoenix et al., 2006;Galloway et al., 2004). Different human activities disturb the natural N cycle in serious ways (Galloway et al., 2004), for example, using artificial fertilizers to increase crop production (Erisman et al., 2008) or excessively relying on fossil fuels for industrial production. N_r production increased from approximately 15 Tg N yr^{-1} in 1860 to 187 Tg N yr^{-1} in 2005 and more than 50% of that N_r has been reported to deposit onto the ground (Nicolas and Galloway, 2008). In the past two decades, high rates of Nr deposition were widely documented in developed countries, such as America (Fenn et al., 1998) and Europe (Dise and Wright, 1995). Great efforts have been made to fight against these negative effects in the USA and the N_{ox} deposition was decreased dramatically in recent years (Li et al., 2016). However, the growing human demand for food and energy at a global scale has resulted in increased emissions of N_r into the environment (Galloway et al., 2008), particularly in large developing countries like China and India (Chen et al., 2019a;Liu et al., 2013).

A nationwide estimate of long-term N deposition in China based on the bulk measurements as well as summaries from reported references in 270 sites by Liu et al. (2013), showed an increasing rate of 0.41 kg N ha^{-1} per year from 1980 to 2010. In contrast to the increasing importance of N_{rd} deposition, due to apparently decreasing N_{ox} resulting from the air quality control policies in the USA in past decades (Li et al., 2016), the ratio of N_{rd}/N_{ox} recorded from bulk/wet deposition decreased from 5:1 in 1980 to 2:1 in 2010. This suggests a more and more important role of N_{ox} in China (Liu et al., 2013). The ratio in highly developed regions such as the North China Plain was even lower than 1:1 in recent years (Pan et al., 2012). However, very limited long-term observations in China challenge our capacity to understand and control the increase of N_r deposition. The published long-term N deposition monitoring network, which includes the Acid Deposition Monitoring Network in East Asia (EANET, http://www.eanet.asia/index.html), the National wide Nitrogen Deposition Monitoring Network (NNDMN) established in 2010 by the China Agriculture University (CAU) (Xu et al., 2015), and the Chinese Ecosystem Research Network (CERN) in North China Plain, established by the Chinese Academy of Science (Pan et al., 2012), the Acid Rain Monitoring Network, run by the China Meteorological Administration (CMA-ARMN) (Tang et al., 2007;Tang et al., 2010;Ge et al., 2011), and the National Acid Deposition Monitoring Network (NADMN) (Li et al., 2019b), have been identified with many shortcomings. Monitoring sites are widely spread over a large

geographical area and therefore data records, due to the high cost of the measurement and unstable financial support, are incomplete. Chemical Transport Model (CTM) simulation is another option to offset these drawbacks and also to quantify long-range transport of deposition in a global or regional map (Seinfeld and Pandis, 2006). It is important to know the accuracy of the CTM before it is employed to investigate the spatial and temporal variation of the depositions. Hayami et al. (2008) and Mann et al. (2014) explain that different parameters in CTMs can result in large variations and the inaccuracies. The multi-model ensemble mean (ENM) shows better performance than any single one (Carmichael et al., 2002;Hayami et al., 2008;Holloway et al., 2008;Wang et al., 2008). Additionally, to better localize applications of CTM, comprehensive evaluations of the strengths and weaknesses of current CTMs for simulating the acid deposition as well as their precursors in a unified framework, with certain regulated rules and the same inputs to models, must be undertaken.

Model Inter-Comparison Study for Asia (MICS-Asia) provides an opportunity to investigate the CTMs application with different models in Asia. MICS-Asia was first employed in 1998 with the target of long-range transport and deposition in SO_4^{2-} in the first stage (MICS-Asia phase I) (Carmichael et al., 2002) and sulfur, nitrogen and ozone in the second stage (MICS-Asia phase II) (Carmichael et al., 2008). The findings and methodologies developed in the previous inter-comparison studies contributed to common understandings of the performance and uncertainties of CTM applications in East Asia (Hayami et al., 2008;Carmichael et al., 2008;Han et al., 2008;Wang et al., 2008). The comprehensive multi-model inter-comparison study on acid deposition in China is becoming an urgent issue as the high emissions in China are causing acid deposition in neighboring countries (Lin et al., 2008;Kajino et al., 2011;2013;Itahashi et al., 2018). In this study, one year simulated N_r depositions, i.e. N_{ox} and N_{rd} in both wet and dry deposition, using the framework of MICS-Asia III (MICS-Asia phase III), have been compared with each other and validated by the observed wet deposition from EANET, NNDMN, CREN and by the Department of Ecological Environment (DEE, formerly known as the Environmental Protect Administration, EPA) over the whole of China. The ENM results were also compared to the Vertical Column Density (VCD) from satellite and the emission inventories. Finally, the uncertainties of the sources of N_r depositions and their ecological impacts have been quantified. The results from this study will not only provide an important reference for establishing a suitable N deposition model, the localized application of CTMs in China will also be tested.

2 Framework of intercomparison in MICS-Asia III

2.1 Description of the participant models

In phase III of MICS-Asia, 14 chemical transport models (CTM, M1-M14) were used to compare and evaluate current multi-scale air quality models (called topic 1 in MICS-Asia III). The same number index was used to measure aerosols and ozone levels, reported by Chen et al. (2019b) and Li et al. (2019a). However, the fully coupled online Weather Research and Forecasting model with chemistry (WRF-Chem), which has been indexed as M7-M10, was not included in the deposition comparison part in the overview of model inter-comparison and evaluation

for acid deposition in Asia (Itahashi et al., 2020). Briefly, the Weather Research and Forecasting model coupled with the Community Multi-scale Air Quality (WRF-CMAQ) has been numbered M1-M6, with a different version of v5.0.2 for M1 and M2, v5.0.1 for M3 and v4.7.1 for M4-M6. M11 and M12 are the independent models developed in Japan and China, named as NHM-Chem (Kajino et al., 2019) and the nested air quality prediction model system (NAQPMS), respectively. A global three-dimensional chemical transport model (GEOS-Chem v9.1.3), M13, was also used as the long-range transport and future change prediction model in MICS-Asia III. The last, M14, was represented as the Regional Atmospheric Modeling System coupled with CMAQ (RAMS-CMAQ). It should be noted that the last two models, M13 and M14, were not driven by the "standard" meteorological fields from WRF v3.4.1 model. Basic information about the configuration of each model was summarized in Table 1. More detailed description can also be found in previous studies (Itahashi et al., 2020;Chen et al., 2019b;Li et al., 2019a).

2.2 Model inputs and simulation domain

As mentioned by Chen et al. (2019b), same ("standard") meteorological fields, emission inventories and boundary conditions have been prepared for the CTMs inter-comparison in MICS-Asia III to reduce the uncertainties from model inputs. However, some models such as M13 and M14, imported "non-standard" inputs due to their specific characteristics. The "standard" meteorological inputs were simulated by WRF v3.4.1 with the initial and lateral boundary conditions from the National Centers for Environmental Prediction (NCEP) Final Analysis (FNL) data. Four dimensional data assimilation (FDDA) nudging was adopted every 6 hours to improve the accuracy of the meteorological parameters simulation. The assimilated meteorological fields from the Goddard Earth Observing System 5 (GEOS5) of the US National Aeronautics and Space Administration (NASA) (https://gmao.gsfc.nasa.gov) were used to drive M13. The M14 model was driven by RAMS with the same FNL data for nudging as the "standard" WRF simulation, which was developed by Pielke et al. (1992). For the emission inputs, all the participant model were using the same emission inventory, which included the MIX anthropogenic emissions over Asia developed for MICS-Asia Phase III (Li et al., 2017), the biogenic emissions calculated by the Model of Emissions of Gases and Aerosols from Nature (MEGAN) version 2.04 (Guenther et al., 2006), and the biomass burning emissions from Global Fire Emission Database (GFED) version 3 (van der Werf et al., 2010). Additionally, SO_2 emissions from volcanoes were collected from the AEROCOM program (https://aerocom.met.no/ DATA/download/emissions/AEROCOM_HC/volc, last access: 11 September 2019, Diehl et al., 2012; Stuefer et al., 2013). MICS-Asia Phase III provided two sets of lateral boundary conditions derived from GEOS-Chem (Bey et al., 2001) and CHASER (Sudo et al., 2002), respectively. The boundary conditions from GEOS-Chem were run with 2.5 °×2 ° resolution and 47 vertical layers, while those from CHASER were run with 2.8 °×2.8 ° and 32 vertical layers. M4, M5, M6, M11 and M12 used the output from CHASER as the boundary conditions, and M1, M13 and M14 were from GEOS-Chem. Only M2 used the default boundary condition field provided in CMAQ.

The "standard" simulation domain covers the region of East Asia (15.4 °S-58.3 °N, 48.5 °-160.2 °E) with 180×170 grids at 45 km horizontal resolution. M1-M6, M11 and M12 followed "standard" simulation domains, while M13 and M14 employed different modeling domains with 0.5 ° latitude × 0.667 ° longitude and 64 × 64 km, respectively. In this study, the analyzed region was only focused in China and all participant models covered it. Therefore, simulated reactive N depositions in each model can be analyzed and compared to show the performance of the participant models. All models output of N depositions have been classified as oxidized N (N_{ox} = $gHNO_3$ + gNO_x + pNO_3^-, including gaseous nitrate acid, NO_x and particulate nitrate) and reduced N (N_{rd} = gNH_3 + pNH_4^+, including gaseous ammonia and particulate ammonium) for comparison. Several previous studies have reported that the contributions of the other N species, e.g., PAN and isoprene nitrates to total N dry deposition are less important than the inorganic N, e.g., HNO_3 and NO_x (Yuan et al., 2018; Wolfe1 et al., 2011; Wolfe1 et al., 2011). Thus, these organic N species were not included in this study.

2.3 Observation data

China has a large land mass - almost 5,500 km from south to north (3.5 °-53.3 °N) and 5,200 km from west to east (75.5 °-135 °E). It goes from coastal to inland and from a tropical climate to a frigid zone. Only 8 sites located in Guangdong, Fujian, Sichuan and Shanxi in EANET were insufficient to show the real performance of CTMs in China. Besides the 8 EANET sites, data from 83 sites recorded daily, weekly or yearly from the CERN (Pan et al., 2012), NNDMN (Xu et al., 2015; Liu et al., 2013) and DEE in Guangdong, Liaoning and Xinjiang province and Shanghai were employed in this study to compare the simulated wet deposition in MICS-Asia III in China. Figure 1 shows the location of the 83 measurement sites as well as the divided regions of the whole of China. There were 50 urban sites and 33 rural sites. More detailed information of each measurement site can also be found in Table S1 in the supplementary documents.

The daily wet deposition was measured by a wet-only sampler to collect precipitation samples during the rainfall event in EANET. Analysis methods for NO_3^- and NH_4^+ were based on ion chromatography and checked by ion balance and conductivity agreement. Detailed descriptions can be found in the source document (EANET, 2010). Daily rainwater samples at 10 sites located in the North China Plain were collected using a custom wet-dry automatic collector (APS-2B, Xianglan Scientific Instruments Co., Ltd., Changsha, China) in CREN. Inorganic N, including NO_3^- and NH_4^+, in the precipitation samples was measured using an ion chromatography system (Model ICS- 90, Dionex Corporation, Sunnyvale, CA, USA) and the standard laboratory procedure of LAPC (Wang et al., 2012). The detection limit (DL) of N for this instrument was 5 μg l^{-1}. A detailed description can be found in the research of Pan et al. (2012). The wet/bulk NO_3^- and NH_4^+ deposition data from 25 sites of China Agricultural University Deposition Network (CAUDN), which was renamed as NNDMN in China in 2010, has been collected and reanalyzed as yearly data (Xu et al., 2015;Liu et al., 2013). At all monitoring sites precipitation samples were collected using precipitation gauges (SDM6, Tianjin Weather Equipment Inc.,

China) located beside the DELTA systems (ca. 2m, DEnuder for Long-Term Atmospheric sampling). After their collection, the samples were analyzed in CAU's laboratory based on the standard laboratory procedure of CAU (Xu et al., 2015). Routine NO_3^- and NH_4^+ wet depositions collected in each rainfall event at 40 sites were provided by the DEE of Guangdong, Liaoning and Xinjiang provinces as well as Shanghai city. The analytical process was the same used in the laboratory procedure of the China National Environmental Monitoring Centre (CNEMC).

The temporal resolutions of the wet deposition data are different from each other, i.e., daily in EANET and CREN, rainfall event collection in DEE and yearly in NNDMN. For the convenience of comparison, all data from daily or rainfall event collecting samples at each type of measurement site has been summarized and interpolated as monthly wet deposition data to compare with the monthly simulation in MICS-Asia III in this study, except the yearly data provided by NNDMN. VCD of NO_2 from SCIAMACHY (http://www.temis.nl/airpollution/no2col) and NH_3 from IASI (http://ether.ipsl.jussieu.fr/ether/pubipsl/iasial2/iasi_nh3) have also been used to compare with the total deposition as well as the emissions.

3 Results

3.1 Validation of wet deposition

3.1.1 Yearly comparison and monthly variation of oxidized N

Yearly simulated wet deposition of N_{ox} has been evaluated by observed nitrate wet deposition in 83 sites over China. Table 2 lists the statistical parameters of simulated wet deposition of N_{ox} compared with the observed data in rural and urban sites of China. In all sites, M1, M5 and M11 overestimated the yearly wet deposition of N_{ox} with Normalized Mean Bias (NMB) of +30.3%, +55.4% and +67.2%, respectively. M6, M12 and M13 simulated almost comparable results with NMB of -6.8%, +0.6% and +0.1%, respectively. M2, M4 and M14 underestimated the yearly wet deposition of N_{ox} with NMB of -38.7%, -10.7% and -47.4%, respectively. The NME was around 50% with the highest 82.2%, in M11, which is lower than that reported over the East Asia with the value of 70% based on EANET observation by Itahashi et al. (2020). However, the correlation coefficient R was around 0.2~0.3 (n=83) which is lower than the East Asia comparison based on the EANET data (0.3~0.4, n=54) (Itahashi et al., 2020). In order to eliminate influences from rainfall uncertainties (R=0.82), the volume weighted mean (VWM) concentration of N_{ox} in precipitation has also been evaluated. In contrast to the low R value of yearly wet deposition of N_{ox}, the correlation R increased to almost 0.5 for the VWM concentrations. To judge the agreement between simulation and observation, the percentages within a factor of 2 (FAC2) has been calculated in this study. Approximately 50% of model results corresponded within the percentages within FAC2. M1 and M13 showed better agreement with 60% and 59% within FAC2, while M2 and M14 showed only 36% and 45% agreement within FAC2. The ground surface measurement sites were divided into 49 urban sites and 34 rural sites according to their location. Overall, all the models showed better performance with the R in 0.2~0.4 and FAC2 in 50%~60% in urban sites than that of R in 0.05~0.3 and FAC2 in 40%~50% in rural sites. This difference may not be due to the uncertainties in rainfall simulation, as the simulated

VWM concentration of N_{ox} in precipitation may eliminate the rainfall uncertainties, and also shows better agreement in urban locations than that in rural sites (Table 2).

Figure 2 shows the percentile box plot the yearly wet deposition of N_{ox} simulated by 9 participant models in five regions of China (i.e., North China (NC), Northeastern China (NE), southeastern China (SE), northwestern China (NW), southwestern China and Tibet Plateau (SW+TP)). Site by site validation of both the yearly wet deposition and VWM concentration of N_{ox} simulated by each model are also displayed in Figure S1. The model results show large intra-region or inter-region uncertainties, especially in NC, NE and SE. The highest wet deposition of N_{ox} simulated by M11 is almost 3~4 times the lowest result simulated by M14 in the above regions (Figure 2). Specifically, two models simulate 30-50% higher N_{ox} wet deposition, while four models are 20~40% lower compared to the averaged observations in NC with the averaged value 6.5 kg N ha^{-1} a^{-1}. For the wet deposition of N_{ox} in SE and SW+TP, most of the participant models are more than 50% underestimated with the largest underestimation of 75% from M14, even though the precipitation in this region is overestimated. Additionally, the divergence of observed N_{ox} wet deposition between different sites in NC, SE and SW, which was shown as the length of the red box in Figure 2a, 2d and 2e, is significantly larger than the multi-models' results. The scattered distribution of the measurement sites in these regions is responsible for the large divergence in observations. However, most of the participant models failed to capture the large difference, indicating that the coarse grid in MICS-Asia III (45 km) is not suitable for the performance of detailed characterization at a local scale. A global assessment of the ensemble simulated wet depositions in the Task Force on Hemispheric Transport of Atmospheric Pollutants (TF HTAP) by Vet et al. (2014) also indicated the underestimation of the models in a number of sites in North America, Europe, Central Africa and part of East Asia. The under-prediction in Europe was found due to the large under-predictions of precipitation depth, while the reason for the error in East Asia is still unknown. However, most of the models overestimate the wet deposition of N_{ox} in NE. Several models including M1, M5 and M11 simulate more than 10 kg N ha^{-1} a^{-1} N_{ox} wet deposition, almost double the observed value of 5 kg N ha^{-1} a^{-1}. Both the multi-models and the observations show very low values of 3-4 kg N ha^{-1} a^{-1} N_{ox} wet deposition in NW, where the precipitation depth was very low compared to the other regions of China (Figure S1).

Regarding to the comparison over the whole of East Asia reported in the overview of acid deposition in MICS-Asia III (Itahashi et al., 2020), similar overestimation was found in M5 and M11 while underestimation in M2, M4 and M14. It should be noted that the EANET sites are mostly located around Japan, Korea and Southeast Asia, and only 8 sites are located in China. The similar performances between the validation in East Asia and China indicated the general underestimation (overestimation) of M2, M4 and M14 (M5 and M11) were reliable in these models. For the rest of models, different results were found between China and East Asia, i.e., the simulated N_{ox} wet deposition in M1 was significant overestimated in China (Figure 6 of Itahashi et al., 2020), but comparable with the observations over the rest of East Asia. Due to the absence of the observations for atmospheric NO_2/NO_3^-, we cannot validate their

model performances directly. Instead, another companion paper (Chen et al., 2019b) reported that most of models overestimated NO_3^- concentrations based on 14 sites in China with most sites located in NC (Figure S5 of Chen et al., 2019b). In summary, the relationship between the atmospheric concentration of NO_3^- and the wet deposition in NC was not obvious, which is also same as that found in East Asia (Itahashi, et al., 2020).

Further evaluations in temporal variations both in urban and rural sites of NC and NE are displayed in Figure 3. Generally, all of the models and observations found high levels of depositions in spring and summer and low values in winter in the two regions. High depositions were due to large precipitation depth in the rainy season. However, this was not always true in some urban sites. For example, higher depositions of N_{ox} were observed in May and June with lower rainfall volume than in July and August with higher rainfall in the urban sites of NC. Similar examples were found at urban sites in NE. Previous studies confirmed there is a decreasing trend in variations of chemical components in precipitation as rainfall varies (Aikawa and Hiraki, 2009;Aikawa et al., 2014;Xu et al., 2017). If the rainfall lasts long enough, or if rainfall volume was large enough, the concentrations of chemical components in precipitation remained at low levels and were attributed to the effects of the in-cloud scavenging process. That is, the large rainfall in an event may not cause the high level of monthly wet depositions due to the low level of in-cloud deposition compared to the wet depositions by several different precipitation events, especially in polluted regions in urban sites. Unfortunately, only monthly data of wet depositions and precipitation have been compared in this MICS-Asia III. Detailed comparisons of rainfall events should be considered in the future.

3.1.2 Yearly comparison and monthly variation of reduced N

Simulated wet deposition of N_{rd} in MICS-Asia III has been evaluated using multi-source observations from the same sites referred to in N_{ox}. It is shown in Table 3 that all of the models underestimated the N_{rd} wet depositions with the negative NMB both in urban and rural sites. Although little difference between rural and urban sites was found in M11 and M14, a better performance in rural areas was manifested by lower NMB and higher FAC2 in rural sites than the urban sites in most of models (-13.6%~-23.2% vs -37.3%~-45.6% for NMB and 55.9-70.6% vs 42.9-55.1% for FAC2, except M11 and M14). The underestimation of the simulated N_{rd} wet depositions was also found in the VWM concentration of N_{rd} in precipitation with similar NMB and FAC2. However, compared with the wet deposition, the correlation between the simulated and observed N_{rd} VWM concentration in precipitation was significant with the R increased from ~0.3 to ~0.8, which was similar with that shown in N_{ox}. This indicates the simulated VWM concentration of N_{rd} in precipitation by MICS-Asia III has better performance in spatial variation than the simulation of N_{rd} wet deposition over China.

The underestimation of N_{rd} wet deposition was also found over the whole of East Asia reported in the overview of acid deposition in MICS-Asia III (Itahashi et al., 2020). This implies the current CTM models might underestimate prediction of N_{rd} wet deposition not only in China but also in the whole of East Asia. The close

correlations between the atmospheric concentration of NH_4^+ and wet deposition of N_{rd} with overestimation in the atmosphere but underestimation in precipitation were found over all of East Asia (Itahashi et al., 2020). In this study, the consistent relationships in NC were also found in the results of Chen et al. (2019b) (overestimated NH_4^+ concentration) and in this study (underestimated N_{rd} wet deposition). Bae et al. (2012) reported the below-cloud scavenging process was important in the simulation of N_{rd} wet deposition, which was not explicitly separated in-cloud and below-cloud scavenging but computes it as a whole in the CMAQ model. Note that the wet scavenging process in most of models (including M11 and M12) of MICS-Asia III were similar with that treated in CMAQ module except M13 (Table 1). It is too simple to accurately simulate wet deposition with the absence of accurate below cloud wet scavenging simulation. This would be one reason for the underestimation of N_{rd} wet deposition, especially considering the high concentration of gaseous ammonia in the surface layer of NC (Pan et al., 2018; Kong et al., 2019).

Specifically, the performance of N_{rd} wet deposition prediction in MICS-Asia III has also been validated in five regions through the percentile box plot in Figure 4. Site by site validation of both the yearly wet deposition and VWM concentration of N_{rd} simulated by each model are displayed in Figure S2. Different from that found in N_{ox}, almost similar behavior prediction has been found in same models, i.e., CMAQ models in M1~M6, except M12, which was driven by a different meteorological model. Other regional models as well as a global model show significantly different percentile distributions in all regions. Overall, both the medium and mean value of N_{rd} wet deposition were underestimated in NC, SE and SW+TP, while they are found to be similar in NE and NW. The underestimation in NC was largely due to the under prediction in summer time not only in urban sites (Figure 3e) but also in rural sites (Figure 3f). Unfortunately, we cannot obtain convincing temporal variations in SE and SW since the scarcely of monthly data in these two regions – there being only one or two sites in each region. In NE, most models predicted similar temporal variations of N_{rd} wet deposition, especially the high depositions in the summer months.

3.2 Map of wet deposition among participant models

3.2.1 Wet deposition of oxidized N

Figure 5 shows the map of the distribution of yearly N_{ox} wet deposition simulated by each participant model, the ENM results and the observed results over China. Most models show similar spatial patterns, with high levels of depositions in central to eastern China and low levels in western China. However, the threshold value in the hotspot areas (from light yellow color to orange and red colors) varies significantly among the models and the average is much higher than the Nr deposition threshold value of 10 kg N ha^{-1} to the temperate ecosystems suggested by Bleeker et al.(2011). For example, M1, M5 and M11 simulated very high wet depositions of N_{ox} (almost reaching at 20 kg N ha^{-1}) in the middle Yangtze River and Yangtze River Delta (YRD), basin of Sichuan Province, south of NC and Liaoning Province located in NE. In contrast, M2 and M14 fail to show the relative hotspot N_{wox} in such areas, and M4,

M6, M12 and M13 show an obscure hotspot with a small value of 10 kg N ha^{-1}. The significant differences not only exist between different models but also in the same model CMAQ, i.e., M1, M2, M4, M5 and M6. Since most models were driven by the meteoroidal field and standard emission input except M13 (Geos-Chem) and M14 (RAMS-CMAQ), the differences in simulated N_{ox} wet deposition should come from the CTMs themselves, such as the diffusion and convection process, the oxidation and chemical transformation as well as the wet scavenging and deposition processes. The comparison of the long lifetime specie CO (Kong et al., 2019) and weak chemical activity specie BC (Chen et al., 2019b) revealed that the model uncertainties are less than other factors, i.e., O_3 (Li et al., 2019) and NO_3^- (Chen et al., 2019b) which have strong chemical activity and short lifetimes in the atmosphere. These results indicate that the chemical reaction process rather than the diffusion and convection process is one of the most important factors affecting the model uncertainties in MICS-Asia III.

3.2.2 Wet deposition of reduced N

Figure 6 shows the map distribution of the reduced N (N_{rd}) wet deposition over China. All of the models show a similar spatial pattern with high values in central and eastern China but low level of deposition in NW and northwestern of NE. Compared with the N_{ox}, few differences of the simulated N_{rd} wet deposition were found among 9 models except M11, which predicted significantly lower values. N_{ox} wet deposition of five agricultural dominant provinces - Shandong, Henan, Hubei, Hunan and Anhui - is higher than the threshold value of 10 kg N ha^{-1}, according to the simulated results by most models. Unfortunately, the small number of observations in these areas make it harder to validate their findings. Evidence shows the high level of N_{rd} wet deposition over the threshold based on the observations in Hebei, YRD and Pearl River delta (PRD). Almost all of the models under-predicted in these areas. Liu et al. (2013) reported the important contribution of N_{rd} to the total N deposition in China based on the long-term national scale of observed nitrogen deposition data. In the agricultural predominantly agricultural areas, ammonia emission is the main contributor to N_{rd} deposition (Liu et al., 2011 AE review; Kang et al., 2016).

3.3 Comparisons among participant models for reactive N depositions

3.3.1 Coefficient of variations for N depositions in MICS-Asia III

Besides the wet deposition of oxidized and reduced N, dry deposition was also an important process for the total deposition in China (Liu et al., 2013;Pan et al., 2012). Coefficient of Variation (hereinafter, CV), defined as the standard deviation divided by mean value of all selected model results, with a large value denoting lower consistency among the models, is applied for model comparison of simulated reactive N depositions both for dry and wet deposition processes in MICS-Asia III. Figure 7 shows the distribution of CV for each type of simulated reactive N deposition. Since the low level of mean values of deposition are more likely to be associated with a higher CV, the gridded CV was only calculated in the area with the simulated depositions higher than 0.5 kg N ha^{-1} (hereafter, analyzed value) in this study. As shown in Figure 7, the spatial distribution of CV only covers Eastern China, Southern China and Northeast China, which indicate that the quarterly and yearly fluxes of reactive N deposition in these regions was higher than the analyzed value. For the

annual case, the CV value of N_{rd} was lower compared with N_{ox} both for dry and wet depositions. This means the multi-model simulations are more consistent in N_{rd} depositions than in N_{ox} depositions. Specifically, the N_{rd} in wet depositions have the lowest CV values, followed by N_{rd} in dry depositions and then the N_{ox} in wet and dry depositions. This suggests the simulated wet depositions of N_{rd} have fewer uncertainties than other types of reactive N depositions.

More complicated patterns were shown in seasonal variations of each type of deposition. The simulated N_{ox} for dry deposition in Figure 7 (a) showed larger uncertainties in southern China (south of 30 ℃N, with the CV > 0.4) than that in northern China (north of 30 ℃N, with the CV <0.3) in all seasons except summer. Similar spatial and temporal patterns of the CV values were found in N_{rd} dry deposition. It is worth noting that the large CV values with the range of 0.4-0.6 were exhibited in Central China (i.e., Henan, Hebei and Shandong provinces) during summer and autumn in spite of the high flux of N_{rd} dry depositions in these regions (Map distributions of N_{ox} and N_{rd} dry depositions, simulated in 9 participant models, is displayed in Figure S3 and Figure S4 of the supplementary documents). This suggests, importantly, that the uncertainties of the physical and chemical processes in the participant models - including gas-particle equilibrium (Ge et al., 2019), dry deposition parameter scheme (Zhang et al., 2003), transportation as well as the chemical reaction with other acidifying substances (Liu et al., 2019) - in the regions of high emissions originating from agricultural activities in growing seasons may lead to significant deviations of simulated N_{rd} dry depositions.

For wet deposition of N_{ox}, large uncertainties were located in southern China in summer and autumn with the CV values higher than 0.6 compared with the CV values lower than 0.4 in other regions (Figure 7c). This high value of CV was not found in the summertime of simulated N_{rd} wet deposition (Figure 7d). Due to the high portion of summertime flux to the total annual wet deposition, high CV values in N_{ox} contributed the most important part of the significantly larger annual CV value than that shown in the N_{rd} case. Due to the same rainfall input for the wet deposition in the framework of MICS-Asia III, except model 13 and 14, the different CV values for N_{rd} and N_{ox} in same region (i.e., lower CV values of N_{rd} wet depositions in NC, SE and Central China) can be attributed to their precursor concentrations in the air mass as well as the different wet scavenging processes (Seinfeld and Pandis, 2006). This will be discussed in the following section.

3.3.2 Comparison of precursors in the air mass

As is well known, depositions both from dry and wet parts of a certain substance were found to have originated from its precursor in the air mass. The uncertainties of the nitrogen related species in the air mass simulated during MICS-Asia III were therefore an important index for estimating the performance of deposition simulations. It should be noted that only concentrations of most of the related species at surface layer have been submitted in MICS-Asia III, except NO_2 vertical column density data (VCD). According to the comparison of CV between the NO_2 concentration at the surface layer and VCD data (Figure S5), it was shown that there is a similar spatial pattern over the whole of China. This indicates that the simulated concentration on the

surface layer can partly represent the difference of the whole column among the multi-models, especially in providing a broad overview in China. Thus, only concentration data at the surface layer has been used in this study.

Figure 8 shows the distribution of CV for gaseous NO_x, particulate NO_3^-, gaseous NH_3 and particulate NH_4^+ in the air mass simulated by the 9 participant models during four seasons as well as the annual mean values. There were significant seasonal variations among the spatial patterns of the CV for each type of the N-related air pollutant. It is interesting to note that not only the seasonal variations but also the spatial patterns of the simulated precursors' CV were reasonably consistent with those previously shown in the deposition part (Figure 7). For example, high CV values were found in the simulation of particulate NO_3^- in Southern China during summer, reaching or even exceeding 0.8 in SE China (Figure 8b). The high CV values were also found in summertime N_{ox} wet depositions (Figure 7c). As the most important precursor of N_{ox} wet deposition (Pan et al., 2012), the consistent distribution of CV between the precursor and the deposition is reasonable. Different from the particulate NO_3^-, very low CV values were shown in particulate NH_4^+ during summer leading to less deviation of simulated N_{rd} wet deposition than the N_{ox}. However, uncertainties in precursors cannot explain everything. For example, the high CV values of N_{ox} wet deposition in south China corresponds to the low CV values of NO_3^- in autumn. Some other factors, such as the scavenging process might be responsible for the unknown-uncertainties. Xu et al. (2017;2019) first compared the below-cloud wet scavenging coefficients based on the different estimation methods and found the large difference even at magnitude level between each method. Thus, a more detailed comparison - such as in-cloud and below-cloud wet scavenging coefficients in each participant model - should be carried out in the next phase of MICS-Asia.

For N_{ox} dry depositions, the anomalies of deposition and NO_x concentration in the air are shown in Figure S6 and Figure S7. It shows same variations among the models, i.e., both of higher deposition and concentration in M1, M5, M11, M13, and lower in M2, M4, M6, M12 and M14. This has also been proved in the distribution of CV values in NO_x (Figure 8a) and N_{ox} dry depositions (Figure 7a) during autumn and winter. As the most important precursor of N_{rd} dry deposition, gaseous NH_3 also shows large CV values in central China during summer time (> 0.6). There were also significant high CV values in south of the Yangtze River during the autumn and winter period (0.7-0.8 in south of the Yangtze River vs 0.3-0.5 in north of the Yangtze River). A similar pattern but of uncertain significance was found in the simulated N_{rd} dry deposition (0.3-0.4 vs 0.2-0.3 in Figure 7b). The anomalies of N_{rd} dry deposition and the gaseous NH_3 in the air simulated by each model are shown in Figure S8 and Figure S9. Addintionally, the dry deposition velocity (V_d) of N_{rd} - based on the ratio of the dry deposition fluxes and the surface concentration (same as Tan et al., 2019) - are also shown in Figure S10. The results show that the CMAQ models (M1~M6) predicted similar V_d of N_{rd}, and the N_{rd} dry deposition was consistent with the gaseous NH_3 concentration in the air, i.e., overestimation in M1 and M2 but underestimation in M4 and M5. However, among the different models, high V_d of N_{rd} (low V_d of N_{rd}) was corresponds with the overestimation (underestimation) of dry deposition in M11 and

M14 (M12 and M13). From the distribution of CV, similar patterns were also displayed both in V_d (Figure S11) and dry deposition of N_{rd}, with low CV value in NCP (0.1-0.4 for N_{rd} dry deposition, 0.1-0.3 for V_d) and high CV value in SE and SW (0.4-0.8 for N_{rd} dry deposition, higher than 0.5 for V_d).

4 Discussion

4.1 Ensemble results of reactive N deposition and comparison with satellite data

Wang et al. (2008) first presented the ENM depositions of acidified species over East Asia based on MICS-Asia II simulations and found that the ENM is better in simulating wet depositions than each single model. In the phase III of MICS-Asia, the ENM value of wet depositions both for N_{ox} and N_{rd} has also been validated by observations and shown in Figure 5l and Figure 6l. The simulated N_{ox} wet deposition and VWA concentration in rainfall exhibited larger dispersions around 1:1, in line with the correlation coefficients R of 0.23 and 0.54 in 83 sites over China, compared with those found in N_{rd}, which is concentrated around 1:2 line with the correlation coefficients R of 0.32 and 0.8. This implies the ensemble-mean value of simulated N_{ox} wet deposition has large uncertainties, while N_{rd} wet deposition was under-predicted by a factor of two in MICS-Asia III. Compared to each single model, the ensemble-mean shows a higher R value than most single models. However, due to a lack of direct observation of dry deposition, validation for dry and total deposition of reactive N cannot be achieved. Instead, the column densities from satellite and emissions spatial distribution were employed to address the reasonability of the ensemble-mean of four types of reactive N depositions simulated in nine models. As displayed in Figure 9, dry depositions of N_{ox} and N_{rd} are concentrated in NC, YRD and Henan province, which corresponds to the distribution of their emissions and VCDs, respectively. Meanwhile, wet depositions of N_{ox} and N_{rd} are centered in central China provinces, such as Hubei and Hunan, as well as Chengdu regions. There were especially high wet depositions of N_{rd} in southwest of Hubei province and northeast of Chengdu city, where high values of emissions and the VCDs for NH_3 were absent. These regions loaded with high wet depositions were mainly due to the high volume of rainfall (for more details, see Figure S12) and the long-range transport of acidic substances (Ge et al., 2011).

Another interesting phenomenon is that the allocations of high values of depositions and VCD of N_{ox} are different from that of N_{rd}. As shown in the Figure 9, low depositions with high values of VCD for N_{ox} and high depositions with comparatively lower level of VCD for N_{rd} co-existed in East China. On a global scale, air pollutants must follow the conservation law - that is, the emissions can be divided into two parts, i.e., the depositions and their concentrations in the air. Here we apply this concept to the entire region of China. We assume that the amount of N_{ox} and N_{rd} transported out of the research areas is equivalent under the same atmospheric advection. The emissions of N_{ox} and N_{rd} in China are also comparable (8.3 kg N•ha^{-1} and 8.7 kg N•ha^{-1} for NO_x and NH_3, respectively). At the same time, the simulated low deposition of N_{ox} and observed high VCD match exactly with the high deposition in N_{rd} and observed low VCD in central and eastern China. Although there is no directly observed distribution map to verify the total deposition in our models, the

close correlation between the observed VCD and deposition can verify the rationality of the simulated total deposition distribution.

4.2 Contributions to the total inorganic N depositions and their potential effects

Total inorganic N deposition (TIN), which includes the reduced and oxidized forms of inorganic N deposition both from wet and dry processes, has been calculated for estimating its ecosystem effects in this study as they were measured in most cases before (Pan et al., 2012;Liu et al., 2013). Figure 10 and Figure 11 show the pathway of each type of N deposition to the TIN from a spatial distribution view and 6 regions statistical results, respectively. The ENM dry depositions of gaseous HNO_3 and NH_3 were the two important contributors to the TIN, both of which took part in 18% of TIN over the whole country, while the wet deposition of NO_3^- and NH_4^+ were another two main components with percentages of 23% and 28% (Table 4), respectively. Consistent with that reported in the global assessment under HTAP (Vet et al., 2014) and in the nationwide monitoring network (NNDMN) estimation (Xu et al., 2015), the N_{rd} in China dominated the TIN deposition with the average percentage reached at 52% for the ensemble results, which is slightly lower compared with 60% and 58% in the two previous works. The overall contribution of wet and dry deposition to TIN was almost half and half, which is consistent with that reported in NNDMN by Xu et al. (Xu et al., 2015). Considering total emissions, the depositions in all of China took about 67%, 65% and 66% in the 2010 emission of NH_3, NO_x and total N (NH_3-N+NO_x-N), respectively. It is interesting to show that the relationship of the gridded average N_{rd} deposition and the N_{ox} deposition with their relevant emissions in six regions (shown in Figure 12 with the slope: 0.56, r^2:0.97 for N_{rd} and the slope: 0.47, r^2:0.88 for N_{ox}) were consistent with that reported by Xu et al. (Xu et al., 2015) (slope: 0.51, r^2:0.89 for N_{rd} and slope: 0.48, r^2:0.81 for N_{ox}). Even the increasing order of the regions from lowest in TP to highest in NC was the same as the previously measurement study. This implicates the spatial distribution as well as the relationships of deposition and emission are comparable with that measured in the NNDMN. Pan et al. (2013) also compared the correlations between the observed depositions and emissions and attributed the inconsistent distribution between them in NCP to the uncertainties of the emission. However, the patterns of depositions were also influenced by the regional transport in addition to the emissions. In this study, significant positive correlations of the simulated N_{ox}(N_{rd}) depositions with the corresponding NO_x(NH_3) emission reflects the control role of the relative emission to the spatial distribution of the depositions. Although most regions were located below a 1:1 ratio of deposition to emission (Figure 12), a few regions, such as TP and NE, were close to or above 1:1 ratio, implicating the impacts of transport on deposition among the regions.

For regions, the area-average deposition of TIN was as highest as 29.2 kg N•ha^{-1} and 27 kg N•ha^{-1} in NC and SE, followed by 15 kg N•ha^{-1} and 10.1 kg N•ha^{-1} in SW and NE, respectively. The TIN in NW and TP were as low as 3.1 and 2.7 kg N•ha^{-1}. In the two highest regions of NC and SE, the deposition of TIN was similar but the pathways to them were different. The N_{rd} deposition (53%) and the dry deposition (54%) contributed more than half the TIN in NC, while the N_{ox} deposition (55%)

dominated the TIN in SE. Considering the lower ratio of NO_x/NH_3 emission in SE (21.4/21.6, 0.99) than NC (30.4/24.4, 1.25), higher contribution of N_{ox} to TIN in SE indicated a higher nitrogen oxidant ratio (i.e., the ratio of oxidation from NO_2 to NO_3^-) than NC. Our companion paper (Tan et al., 2019) also revealed the higher nitrogen oxidation ratio in SE as 0.4-0.6, compared with that in NC as 0.2-0.4. For more oxidant N species, i.e., HNO_3 and NO_3^-, both dry and wet depositions were higher in SE than that shown in NC (5.8 vs. 4.9 for dry deposition of gaseous HNO_3 and 6.9 vs. 6.3 for wet deposition of particulate NO_3^-). While for less oxidant N and the reduced N, all types of depositions - such as dry deposition of gaseous NO_x, gaseous NH_3 as well as the particulate NH_4^+ - were less in SE than NC, except the wet deposition of particulate NH_4^+, due to the much higher volume of rainfall in SE (Figure S5). Overall, the oxidant N made the emitted NO_x easier to scavenge in SE with the ratio of N_{ox}-deposition/NO_x-emission reaching 70%, while the reduced N is more likely to be scavenged from its emission with the ratio of 64% in NC. The total ratio of TIN/emission in NC and SE were 53% and 63%, respectively. Compared to the Critical Load (Duan et al., 2001;Zhao et al., 2009;Liu et al., 2011), which is a judgement of the deposited N effects to the ecosystem, the two regions almost reached in some cases and even exceeded to the CL value (Table 4), indicating serious ecological impacts of the N deposition in NC and SE. More attention should be given to controlling N related species, especially the N_{rd} in NC and N_{ox} in SE.

In the less developed economic and social area of SW, due to the high emission of NH_3, 60% of the TIN was contributed by N_{rd} deposition. The ratio of NO_x/NH_3 emission reached 0.49 as more NH_3 was emitted from agricultural activity than NO_x from fossil fuel consumption. The ratio of wet deposition/TIN was 55%, which was lower than the HTAP comparison during 2000 (60-70%) (Vet et al., 2014), but higher than the results of NNDMN (45%) (Xu et al., 2015). Although socially undeveloped, the TIN deposition was almost as high as the CL value, according to Zhao et al. (Zhao et al., 2009). Besides, the high emission of NH_3, the high ratio of N_{ox}-deposition/NO_x-emission of up to 94% reflects the importance of N_{ox} from high emission areas, such as SE and NC, should attract our attention in this region. Although the N deposition in TP was not as high as CL value - which was the lowest in all regions of China with the value of 2.7 kg N•ha^{-1} - the N ecological impacts cannot be neglected since the sensitive ecosystem (Shen et al., 2019) as well as the important climatic influence to all of China. Considering the high ratio of TIN/emissions, which were larger than 1:1 - with 3:1 for TIN, 2.71:1 for N_{rd} and 4:1 for N_{ox} - the imports from outside the region were responsible for the N deposition in TP.

5 Conclusion

Reactive N depositions over China simulated in the frame work of MICS-Asia III have been compared within each participant model. Wet depositions were also validated by multi-source observations, i.e., recorded data from EANET, CAS, NNDMN and EPA in Guangdong and Liaoning province. Most models show the consistent spatial and temporal variation of both N_{ox} and N_{rd} wet depositions in China with the NME around 50%, which is lower than the value of 70% based on EANET

observations over Asia. Coefficient of Variation (CV) was applied for model comparison of dry deposition as well as the related precursor's concentration in the air mass. Consistency of both spatial and temporal variation of CV in deposition and the concentration in air mass indicates that performance of the precursors' simulation was highly correlated with their depositions.

Large deposition of ensemble simulation of N_{rd} deposition in eastern China was corresponds with a low level of VCD from satellite measurements, while the case of N_{ox} was just the contrary. The total emission of NO_x and NH_3 was similar at 8 kg $N{\bullet}ha^{-1}$ in China. This indicates the allocation of both NO_x and NH_3 from the deposition to the surface ground and the amount staying in the atmosphere were conserved from their emission into the air, which also implicates the reasonable simulation of depositions for N_{ox} and N_{rd} in MICS-Asia III.

Wet deposition of nitrate and ammonium as well as the dry deposition of Gaseous NH_3 and HNO_3 were the important pathway to TIN deposition with the percentages of 18%, 18%, 23% and 28% for ensemble results, respectively. The gridded averaged N_{rd} in China dominated the TIN deposition with the average percentage found to be 52%, which is slightly lower than the reported 60% and 58% in HTAP and NNDMN measurements. The contribution of wet and dry deposition to TIN was almost half and half and consistent with that reported in NNDMN. Even the ratio of TIN/emission was similar with the NNDMN, indicating that the spatial distribution as well as the relationships of deposition and emission are comparable with that measured in the NNDMN.

For different regions of China, the simulated N_{ox} wet deposition was overestimated in NE but underestimated in SE and SW, while large uncertainties were shown in NC. Two models simulated 30-50% higher N_{ox} wet deposition, and four models were 20~40% lower compared with observations in NC. The large divergences not only exist between different models but also in the same CMAQ model, i.e., M1-M6. For the simulation of N_{rd} wet deposition, all the models under-predicted in all regions, with the largest underestimation in NC and SE. Different from N_{ox}, almost similar behavior prediction of the less oxidative species such as the N_{rd} wet deposition has been found in CMAQ models, indicating the chemical reaction process is one of the most important factors affecting the model uncertainties in MICS-Asia III. Compared to CL value, the reactive N deposition in NC, SE and SW reached or exceeded the reported CL value and indicates serious ecological impacts. The control of N_{rd} in NC and SW and N_{ox} in SE would be effective to mitigate the TIN deposition in these regions. For the lowest reactive N deposition in TP, however, the N ecological impacts cannot be neglected since it has a sensitive ecosystem and it has an important climatic influence on all of China, especially considering the high ratio of TIN/emission, which was mainly caused by outside sources. The joint prevention and control of air pollution in China should be carefully considered and implemented in the future.

Data availability.

To request observed data for scientific research purposes, please contact Baozhu Ge at the Institute of Atmospheric Physics, Chinese Academy of Sciences, via email (gebz@mail.iap.ac.cn).

Author contribution

BG designed the whole structure of this work, and prepared the manuscript with contributions from all co-authors. BG, SI and KS led the deposition analysis group in MICS-Asia III. DX, JW, FF and QT helped with the data processing. JSF, XW, KY, TN, JL, MK, HL, and MZ performed the model simulations and contributed to submit their simulated deposition results. ZW performed the meteorological model simulation and examined the model performance. ML, JW, JK and QW prepared the emission inventory data. YP and XL supported the observation data in China. ZW was involved in the scientific interpretation and discussion.

Competing interests

The authors declare that they have no conflict of interest

Acknowledgment

We appreciate the Guangdong and Liaoning EPA for providing the observation data of Guangdong and Liaoning province. We also appreciate Mr. Rich Rifkin and Ms. Chuanhong Zhang for the help of the language improvement. This work is supported by the National Natural Science Foundation of China (Grant No 41620104008, 41877313, 41575123, 91744206) and the National Key Research and Development Plan (20017YFC0210100).

Reference:

Aikawa, M., and Hiraki, T.: Washout/rainout contribution in wet deposition estimated by 0.5 mm precipitation sampling/analysis, Atmos Environ, 43, 4935-4939, 2009.

Aikawa, M., Kajino, M., Hiraki, T., and Mukai, H.: The contribution of site to washout and rainout: Precipitation chemistry based on sample analysis from 0.5 mm precipitation increments and numerical simulation, Atmos Environ, 95, 165-174, http://dx.doi.org/10.1016/j.atmosenv.2014.06.015, 2014.

Bae, S. Y., Park, R. J., Yong, P. K., and Woo, J. H.: Effects of below-cloud scavenging on the regional aerosol budget in East Asia, Atmos Environ, 58, p.14-22, 2012.

Benitez, J. M. G., Cape, J. N., Heal, M. R., van Dijk, N., and Diez, A. V.: Atmospheric nitrogen deposition in south-east Scotland: Quantification of the organic nitrogen fraction in wet, dry and bulk deposition, Atmos Environ, 43, 4087-4094, 10.1016/j.atmosenv.2009.04.061, 2009.

Bey, I., Jacob, D. J., Yantosca, R. M., Logan, J. A., Field, B. D., Fiore, A. M., Li, Q. B., Liu, H. Y., Mickley, L. J., and Schultz, M. G.: Global Modeling of Tropospheric Chemistry with Assimilated Meteorology: Model Description and Evaluation, J.geophys.res, 106, 23073–23095, 2001.

Bleeker, A., Hicks, W. K., Dentener, F., Galloway, J., and Erisman, J. W.: N deposition as a threat to the World’s protected areas under the Convention on Biological Diversity, Environ Pollut, 159, 2280-2288, 2011.

Byun, D., and Schere, K. L.: Review of the governing equations, computational algorithms, and other components of the models-3 Community Multiscale Air Quality (CMAQ) modeling system, Appl. Mech. Rev., 59, 51–77, https://doi.org/10.1115/1.2128636, 2006.

Carlton, A. G., Bhave, P. V., Napelenok, S. L., Edney, E. O., Sarwar, G., Pinder, R. W., Pouliot, G. A., and Houyoux, M.: 5 Model representation of secondary organic aerosol in CMAQv4.7, Environ. Sci. Technol., 44(22), 8553–8560, https://doi.org/10.1021/es100636q, 2010.

Carmichael, G. R., Calori, G., Hayami, H., Uno, I., Cho, S. Y., Engardt, M., Kim, S. B., Ichikawa, Y., Ikeda, Y., Woo, J. H., Ueda, H., and Amann, M.: The MICS-Asia study: model intercomparison of long-range transport and sulfur deposition in East Asia, Atmos Environ, 36, 175-199, 2002.

Carmichael, G. R., Sakurai, T., Streets, D., Hozumi, Y., Ueda, H., Park, S. U., Fung, C., Han, Z., Kajino, M., Engardt, M., Bennet, C., Hayami, H., Sartelet, K., Holloway, T., Wang, Z., Kannari, A., Fu, J., Matsuda, K., Thongbooncho, N., and Amann, M.: MICS-Asia II: The model intercomparison study for Asia Phase II methodology and overview of findings, Atmos Environ, 42, 3468-3490, 2008.

Carter, W. L.: Implementation of the SAPRC-99 chemical mechanism into the Models-3 framework, Report to the United States Environmental Protection Agency, available at: http://www.engr.ucr.edu/~carter/pubs/s99mod3.pdf, 2000, last access: 20 March 2019.

Chen, C., Park, T., Wang, X., Piao, S., Xu, B., Chaturvedi, R. K., Fuchs, R., Brovkin, V., Ciais, P., Fensholt, R., Tømmervik, H., Bala, G., Zhu, Z., Nemani, R. R., and Myneni, R. B.: China and India lead in greening of the world through land-use

804 management, Nature Sustainability, 2, 122-129, 10.1038/s41893-019-0220-7,
805 2019a.
806 Chen, L., Gao, Y., Zhang, M., Fu, J. S., Zhu, J., Liao, H., Li, J., Huang, K., Ge, B.,
807 Wang, X., Lam, Y. F., Lin, C. Y., Itahashi, S., Nagashima, T., Kajino, M., Yamaji,
808 K., Wang, Z., and Kurokawa, J.: MICS-Asia III: multi-model comparison and
809 evaluation of aerosol over East Asia, Atmos. Chem. Phys., 19, 11911-11937,
810 10.5194/acp-19-11911-2019, 2019b.
811 Clark, C. M., and Tilman, D.: Loss of plant species after chronic low-level nitrogen
812 deposition to prairie grasslands, Nature, 451, 712-715, 2008.
813 Clark, H., and Kremer, J. N.: Estimating direct and episodic atmospheric nitrogen
814 deposition to a coastal waterbody, Mar Environ Res, 59, 349-366, 2005.
815 Colella, P., and Woodward, P. R.: The piecewise parabolic method (PPM) for gas
816 dynamical simulations, J. Comp. Phys., 54, 174–201, 1984.
817 Dise, N. B., and Wright, R. F.: Nitrogen leaching from European forests in relation to
818 nitrogen deposition, Forest Ecology & Management, 71, 153-161, 1995.
819 Duan, L., Xie, S. D., Zhou, Z. P., Ye, X. M., and Hao, J. M.: Calculation and mapping
820 of critical loads for S, N and acidity in China, Water Air Soil Poll, 130,
821 1199-1204, 2001.
822 Duce, R. A., LaRoche, J., Altieri, K., Arrigo, K. R., Baker, A. R., Capone, D. G.,
823 Cornell, S., Dentener, F., Galloway, J., Ganeshram, R. S., Geider, R. J., Jickells,
824 T., Kuypers, M. M., Langlois, R., Liss, P. S., Liu, S. M., Middelburg, J. J., Moore,
825 C. M., Nickovic, S., Oschlies, A., Pedersen, T., Prospero, J., Schlitzer, R.,
826 Seitzinger, S., Sorensen, L. L., Uematsu, M., Ulloa, O., Voss, M., Ward, B., and
827 Zamora, L.: Impacts of atmospheric anthropogenic nitrogen on the open ocean,
828 Science, 320, 893-897, 10.1126/science.1150369, 2008.
829 EANET: Technical Manual for Wet Deposition Monitoring in East Asia,
830 http://www.eanet.asia/product/manual/techwet.pdf, 2010.
831 Erisman, J. W., Sutton, M. A., Galloway, J., Klimont, Z., and Winiwarter, W.: How a
832 century of ammonia synthesis changed the world, Nat Geosci, 1, 636-639, 2008.
833 Fenn, M. E., Poth, M. A., Aber, J. D., Baron, J. S., Bormann, B. T., Johnson, D. W.,
834 Lemly, A. D., Mcnulty, S. G., Ryan, D. F., and Stottlemyer, R.: NITROGEN
835 EXCESS IN NORTH AMERICAN ECOSYSTEMS: PREDISPOSING
836 FACTORS, ECOSYSTEM RESPONSES, AND MANAGEMENT
837 STRATEGIES, Ecol Appl, 8, 706-733, 1998.
838 Fountoukis, C., and Nenes, A.: ISORROPIA II: A computationally efficient aerosol
839 thermodynamic equilibrium model for K+, Ca2+, Mg2+, NH4+, Na+, SO4 2- ,
840 NO3 - , Cl- , H2O aerosols, Atmos. Chem. Phys., 7, 4639–4659, 2007.
841 Galloway, J. N., Dentener, F. J., Capone, D. G., Boyer, E. W., Howarth, R. W.,
842 Seitzinger, S. P., Asner, G. P., Cleveland, C. C., Green, P. A., Holland, E. A., Karl,
843 D. M., Michaels, A. F., Porter, J. H., Townsend, A. R., and Vorosmarty, C. J.:
844 Nitrogen cycles: past, present, and future, Biogeochemistry, 70, 153-226, 2004.
845 Galloway, J. N., Townsend, A. R., Erisman, J. W., Bekunda, M., Cai, Z. C., Freney, J.
846 R., Martinelli, L. A., Seitzinger, S. P., and Sutton, M. A.: Transformation of the
847 nitrogen cycle: Recent trends, questions, and potential solutions, Science, 320,

889-892, 2008.
Ge, B., Xu, X., Ma, Z., Pan, X., Wang, Z., Lin, W., Ouyang, B., Xu, D., Lee, J., Zheng, M., Ji, D., Sun, Y., Dong, H., Squires, F. A., Fu, P., and Wang, Z.: Role of Ammonia on the Feedback Between AWC and Inorganic Aerosol Formation During Heavy Pollution in the North China Plain, Earth Space Sci, 6, 1675-1693, 10.1029/2019ea000799, 2019.
Ge, B. Z., Wang, Z. F., Xu, X. B., Tang, J., He, Y. J., Uno, I., and Ohara, T.: Impact of the East Asian summer monsoon on long-term variations in the acidity of summer precipitation in Central China, Atmos Chem Phys, 11, 1671-1684, DOI 10.5194/acp-11-1671-2011, 2011.
Guenther, A., Karl, T., Harley, P., Wiedinmyer, C., Palmer, P. I., and Geron, C.: Estimates of global terrestrial isoprene emissions using MEGAN (Model of Emissions of Gases and Aerosols from Nature), Atmos Chem Phys, 6, 3181-3210, 2006.
Han, Z., Sakurai, T., Ueda, H., Carmichael, G. R., Streets, D., Hayami, H., Wang, Z., Holloway, T., Engardt, M., Hozumi, Y., Park, S. U., Kajino, M., Sartelet, K., Fung, C., Bennet, C., Thongboonchoo, N., Tang, Y., Chang, A., Matsuda, K., and Amann, M.: MICS-Asia II: Model intercomparison and evaluation of ozone and relevant species, Atmos Environ, 42, 3491-3509, 2008.
Hayami, H., Sakurai, T., Han, Z., Ueda, H., Carmichael, G. R., Streets, D., Holloway, T., Wang, Z., Thongboonchoo, N., Engardt, M., Bennet, C., Fung, C., Chang, A., Park, S. U., Kajino, M., Sartelet, K., Matsuda, K., and Amann, M.: MICS-Asia II: Model intercomparison and evaluation of particulate sulfate, nitrate and ammonium, Atmos Environ, 42, 3510-3527, 2008.
Holloway, T., Sakurai, T., Han, Z., Ehlers, S., Spak, S. N., Horowitz, L. W., Carmichael, G. R., Streets, D. G., Hozumi, Y., Ueda, H., Park, S. U., Fung, C., Kajino, M., Thongboonchoo, N., Engardt, M., Bennet, C., Hayami, H., Sartelet, K., Wang, Z., Matsuda, K., and Amann, M.: MICS-Asia II: Impact of global emissions on regional air quality in Asia, Atmos Environ, 42, 3543-3561, 2008.
Holtgrieve, G. W., Schindler, D. E., Hobbs, W. O., Leavitt, P. R., Ward, E. J., Bunting, L., Chen, G. J., Finney, B. P., Gregory-Eaves, I., Holmgren, S., Lisac, M. J., Lisi, P. J., Nydick, K., Rogers, L. A., Saros, J. E., Selbie, D. T., Shapley, M. D., Walsh, P. B., and Wolfe, A. P.: A Coherent Signature of Anthropogenic Nitrogen Deposition to Remote Watersheds of the Northern Hemisphere, Science, 334, 1545-1548, 2011.
Holtslag, A. A. M., and Boville, B.: Local versus nonlocal boundary layer diffusion in a global climate model, J. Clim., 6, 1825–1842, 1993.
Itahashi, S., Yumimoto, K., Uno, I., Hayami, H., Fujita, S. I., Pan, Y., and Wang, Y.: A 15-year record (2001–2015) of the ratio of nitrate to non-sea-salt sulfate in precipitation over East Asia, Atmos. Chem. Phys., 18, 2835-2852, 10.5194/acp-18-2835-2018, 2018.
Itahashi, S., Ge, B., Sato, K., Fu, J. S., Wang, X., Yamaji, K., Nagashima, T., Li, J., Kajino, M., Liao, H., Zhang, M., Wang, Z., Li, M., Kurokawa, J., Carmichael, G. R., and Wang, Z.: MICS-Asia III: Overview of model inter-comparison and

evaluation of acid deposition over Asia, Atmos. Chem. Phys., 2019, 1-53, 10.5194/ acp-20-2667-2020, 2020.

Janjic, Z.: The step-mountain eta coordinate model: Further developments of the convection, viscous sublayer, and turbulence closure schemes, Mon. Weather Rev., 122, 927−945, 1994.

Janssens, I. A., Dieleman, W., Luyssaert, S., Subke, J. A., Reichstein, M., Ceulemans, R., Ciais, P., Dolman, A. J., Grace, J., Matteucci, G., Papale, D., Piao, S. L., Schulze, E. D., Tang, J., and Law, B. E.: Reduction of forest soil respiration in response to nitrogen deposition, Nat Geosci, 3, 315-322, 2010.

Kajino, M., Ueda, H., Sato, K., and Sakurai, T.: Spatial distribution of the source-receptor relationship of sulfur in Northeast Asia, Atmos Chem Phys, 11, 6475-6491, 2011.

Kajino, M., Sato, K., Inomata, Y., and Ueda, H.: Source–receptor relationships of nitrate in Northeast Asia and influence of sea salt on the long-range transport of nitrate, Atmos Environ, 79, 67-78, http://dx.doi.org/10.1016/j.atmosenv.2013.06.024, 2013.

Kajino, M., Deushi, M., Sekiyama, T. T., Oshima, N., Yumimoto, K., Tanaka, T. Y., Ching, J., Hashimoto, A., Yamamoto,T., Ikegami, M., Kamada, A., Miyashita, M., Inomata, Y., Shima, S., Ueda, H., Maki, T., and Mikami, M.: NHM-Chem, the Japan Meteorological Agency's regional meteorology – chemistry model (v1.0): model description and aerosol representations, Geosci. Model Dev. Discuss., https://doi.org/10.5194/gmd-2018-128, 2018.

Kajino, M., Deushi, M., Sekiyama, T. T., Oshima, N., Yumimoto, K., Tanaka, T. Y., Ching, J., Hashimoto, A., Yamamoto,T., Ikegami, M., Kamada, A., Miyashita, M., Inomata, Y., Shima, S., Takami, A., Shimizu, A., Hatakeyama, S., Sadanaga, Y., Irie, H., Adachi, K., Zaizen, Y., Igarashi, Y., Ueda, H., Maki, T., and Mikami, M., NHM-Chem, the Japan Meteorological Agency's regional meteorology – chemistry model: model evaluations toward the consistent predictions of the chemical, physical, and optical properties of aerosols, J. Meteor. Soc. Japan, 97(2), 337-374, http://dx.doi.org/10.2151/jmsj.2019-020, 2019.

Kong, L., Tang, X., Zhu, J., Wang, Z., Fu, J. S., Wang, X., Itahashi, S., Yamaji, K., Nagashima, T., Lee, H. J., Kim, C. H., Lin, C. Y., Chen, L., Zhang, M., Tao, Z., Li, J., Kajino, M., Liao, H., Sudo, K., Wang, Y., Pan, Y., Tang, G., Li, M., Wu, Q., Ge, B., and Carmichael, G. R.: Evaluation and uncertainty investigation of the NO2, CO and NH3 modeling over China under the framework of MICS-Asia III, Atmos. Chem. Phys. Discuss., 2019, 1-33, 10.5194/acp-2018-1158, 2019.

Kong, L., Tang, X., Zhu, J., Wang, Z., Pan, Y., Wu, H., Wu, L., Wu, Q., He, Y., Tian, S., Xie, Y., Liu, Z., Sui, W., Han, L., and Carmichael, G.: Improved Inversion of Monthly Ammonia Emissions in China Based on the Chinese Ammonia Monitoring Network and Ensemble Kalman Filter, Environ Sci Technol, 53, 12529-12538, 10.1021/acs.est.9b02701, 2019.

Li, J., Nagashima, T., Kong, L., Ge, B., Yamaji, K., Fu, J. S., Wang, X., Fan, Q., Itahashi, S., Lee, H. J., Kim, C. H., Lin, C. Y., Zhang, M., Tao, Z., Kajino, M., Liao, H., Li, M., Woo, J. H., Kurokawa, J., Wang, Z., Wu, Q., Akimoto, H.,

Carmichael, G. R., and Wang, Z.: Model evaluation and intercomparison of surface-level ozone and relevant species in East Asia in the context of MICS-Asia Phase III – Part 1: Overview, Atmos. Chem. Phys., 19, 12993-13015, 10.5194/acp-19-12993-2019, 2019a.

Li, M., Zhang, Q., Kurokawa, J. I., Woo, J. H., He, K., Lu, Z., Ohara, T., Song, Y., Streets, D. G., Carmichael, G. R., Cheng, Y., Hong, C., Huo, H., Jiang, X., Kang, S., Liu, F., Su, H., and Zheng, B.: MIX: a mosaic Asian anthropogenic emission inventory under the international collaboration framework of the MICS-Asia and HTAP, Atmos. Chem. Phys., 17, 935-963, 10.5194/acp-17-935-2017, 2017.

Li, R., Cui, L., Zhao, Y., Zhang, Z., Sun, T., Li, J., Zhou, W., Meng, Y., Huang, K., and Fu, H.: Wet deposition of inorganic ions in 320 cities across China: spatio-temporal variation, source apportionment, and dominant factors, Atmos. Chem. Phys., 19, 11043-11070, 10.5194/acp-19-11043-2019, 2019b.

Li, Y., Schichtel, B. A., Walker, J. T., Schwede, D. B., Chen, X., Lehmann, C. M., Puchalski, M. A., Gay, D. A., and Jr, C. J.: Increasing importance of deposition of reduced nitrogen in the United States, Proc Natl Acad Sci U S A, 113, 5874-5879, 2016.

Lin, M., Oki, T., Bengtsson, M., Kanae, S., Holloway, T., and Streets, D. G.: Long-range transport of acidifying substances in east Asia - Part II - Source-receptor relationships, Atmos Environ, 42, 5956-5967, DOI 10.1016/j.atmosenv.2008.03.039, 2008.

Liu, M., Huang, X., Song, Y., Tang, J., Cao, J., Zhang, X., Zhang, Q., Wang, S., Xu, T., Kang, L., Cai, X., Zhang, H., Yang, F., Wang, H., Yu, J. Z., Lau, A. K. H., He, L., Huang, X., Duan, L., Ding, A., Xue, L., Gao, J., Liu, B., and Zhu, T.: Ammonia emission control in China would mitigate haze pollution and nitrogen deposition, but worsen acid rain, Proceedings of the National Academy of Sciences, 116, 7760, 10.1073/pnas.1814880116, 2019.

Liu, X. J., Duan, L., Mo, J. M., Du, E. Z., Shen, J. L., Lu, X. K., Zhang, Y., Zhou, X. B., He, C. N., and Zhang, F. S.: Nitrogen deposition and its ecological impact in China: An overview, Environ Pollut, 159, 2251-2264, 2011.

Liu, X. J., Zhang, Y., Han, W. X., Tang, A. H., Shen, J. L., Cui, Z. L., Vitousek, P., Erisman, J. W., Goulding, K., Christie, P., Fangmeier, A., and Zhang, F. S.: Enhanced nitrogen deposition over China, Nature, 494, 459-462, 2013.

Liu, H., Jacob, D. J., Bey, I., and Yantosca, R. M.: Constraints from ^{210}Pb and ^{7}Be on wet deposition and transport in a globalthree-dimensional chemical, J. Geophys. Res., 2001, 106(D11), 12109–12128, 2001.

Mann, G. W., Carslaw, K. S., Reddington, C. L., Pringle, K. J., and Henzing, J. S.: Intercomparison and evaluation of global aerosol microphysical properties among AeroCom models of a range of complexity, Atmospheric Chemistry & Physics, 14, 4679-4713, 2014.

Nenes, A., Pandis, S.N., and Pilinis, C.: ISORROPIA: A new thermodynamic equilibrium model for multiphase multicomponent inorganic aerosols, Aquat. Geoch., 4, 123–152,1998.

Nicolas, G., and Galloway, J. N.: An Earth-system perspective of the global nitrogen

cycle, Nature, 451, 293-296, 2008.
Pan, Y. P., Wang, Y. S., Tang, G. Q., and Wu, D.: Wet and dry deposition of atmospheric nitrogen at ten sites in Northern China, Atmos Chem Phys, 12, 6515-6535, 2012.
Pan, Y., Tian, S., Zhao, Y., Zhang, L., Zhu, X., Gao, J., Huang, W., Zhou, Y., Song, Y., and Zhang, Q.: Identifying ammonia hotspots in China using a national observation network, Environ Sci Technol, 2018.
Phoenix, G. K., Hicks, W. K., Cinderby, S., Kuylenstierna, J. C. I., Stock, W. D., Dentener, F. J., Giller, K. E., Austin, A. T., Lefroy, R. D. B., Gimeno, B. S., Ashmore, M. R., and Ineson, P.: Atmospheric nitrogen deposition in world biodiversity hotspots: the need for a greater global perspective in assessing N deposition impacts, Global Change Biol, 12, 470-476, 2006.
Pielke, R. A., Cotton, W. R., Walko, R. L., Tremback, C. J., Lyons, W. A., Grasso, L. D., Nicholls, M. E., Moran, M. D., Wesley, D. A., Lee, T. J., and Copeland, J. H.: A comprehensive meteorological modeling system—RAMS, Meteorol Atmos Phys, 49, 69-91, 10.1007/BF01025401, 1992.
Pleim, J. E., Xiu, A., Finkelstein, P. L., and Otte, T. L.: A coupled land-surface and dry deposition model and comparison to field measurements of surface heat, moisture, and ozone fluxes. Water Air Soil Pollut. Focus, 1(5), 243–252, https://doi.org/10.1023/A:1013123725860, 2001.
Pleim, J. E.: A combined local and nonlocal closure model for the atmospheric boundary layer, Part I: Model description and testing, J. Appl. Meteor. Climatol., 46, 1383–1395, 2007a.
Pleim, J. E.: A combined local and nonlocal closure model for the atmospheric boundary layer. Part II: Application and evaluation in a mesoscale meteorological model, J. Appl. Meteorol. Clim., 46, 1396–1409, 2007b.
Seinfeld, J. H., and Pandis, S. N.: Atmospheric chemistry and physics: from air pollution to climate change, Wiley, New York, 2006.
Shen, H., Dong, S., Li, S., Xiao, J., Han, Y., Yang, M., Zhang, J., Gao, X., Xu, Y., Li, Y., Zhi, Y., Liu, S., Dong, Q., Zhou, H., and Yeomans, J. C.: Effects of simulated N deposition on photosynthesis and productivity of key plants from different functional groups of alpine meadow on Qinghai-Tibetan plateau, Environ Pollut, 251, 731-737, https://doi.org/10.1016/j.envpol.2019.05.045, 2019.
Sudo, K., Takahashi, M., Kurokawa, J. I., and Akimoto, H.: CHASER: A global chemical model of the troposphere 1. Model description, Journal of Geophysical Research, 107, ACH-1-ACH 7-20, 2002.
Tang, J., Chen, H. B., Yu, X. L., Wang, S., Yao, P., Lv, B., Xu, X. B., and Ding, G.: Evaluation of results of station inter-comparison with blind samples in Acid Rain Monitoring Network in China(in Chinese), Meteoro. Monthly, 33, 75–83, 2007.
Tang, J., Xu, X., Ba, J., and Wang, S.: Trends of the precipitation acidity over China during 1992-2006, Chinese Sci Bul, 5, 1-9, 2010.
Tan, J., Fu, J. S., Carmichael, G. R., Itahashi, S., Tao, Z., Huang, K., Dong, X., Yamaji, K., Nagashima, T., Wang, X., Liu, Y., Lee, H. J., Lin, C. Y., Ge, B., Kajino, M., Zhu, J., Zhang, M., Hong, L., and Wang, Z.: Why models perform differently on

particulate matter over East Asia? – A multi-model intercomparison study for MICS-Asia III, Atmos. Chem. Phys. Discuss., 2019, 1-36, 10.5194/acp-2019-392, 2019.

van der Werf, G. R., Randerson, J. T., Giglio, L., Collatz, G. J., Mu, M., Kasibhatla, P. S., Morton, D. C., DeFries, R. S., Jin, Y., and van Leeuwen, T. T.: Global fire emissions and the contribution of deforestation, savanna, forest, agricultural, and peat fires (1997–2009), Atmos. Chem. Phys., 10, 11707-11735, 10.5194/acp-10-11707-2010, 2010.

Vet, R., Artz, R. S., Carou, S., Shaw, M., Ro, C. U., Aas, W., Baker, A., Bowersox, V. C., Dentener, F., Galy-Lacaux, C., Hou, A., Pienaar, J. J., Gillett, R., Forti, M. C., Gromov, S., Hara, H., Khodzher, T., Mahowald, N. M., Nickovic, S., Rao, P. S. P., and Reid, N. W.: A global assessment of precipitation chemistry and deposition of sulfur, nitrogen, sea salt, base cations, organic acids, acidity and pH, and phosphorus, Atmos Environ, 93, 3-100, 2014.

Walcek, C. J., and Aleksic, N. M.: A simple but accurate mass conservative peak-preserving, mixing ratio bounded advection algorithm with fortran code, Atmos. Environ., 32, 3863–3880, 1998.

Wang, Y., Yu, W., Pan, Y., and Wu, D.: Acid neutralization of precipitation in Northern China, J Air Waste Manag Assoc, 62, 204-211, 2012.

Wang, Y. X., McElroy, M. B., Jacob, D. J., and Yantosca, R. M.: A nested grid formulation for chemical transport model over Asia: Applications to CO, J. Geophys. Res., 109, D22307, https://doi.org/10.1029/2004JD005237, 2004.

Wang, Z. F., Xie, F. Y., Sakurai, T., Ueda, H., Han, Z. W., Carmichael, G. R., Streets, D., Engardt, M., Holloway, T., Hayami, H., Kajino, M., Thongboonchoo, N., Bennet, C., Park, S. U., Fung, C., Chang, A., Sartelet, K., and Amann, M.: MICS-Asia II: Model inter-comparison and evaluation of acid deposition, Atmos Environ, 42, 3528-3542, 2008.

Wesely, M. L.: Parameterization of surface resistance to gaseous dry deposition in regional numerical models, Atmos. Environ., 16, 1293–1304, 1989.

Wolfe, G. M., Thornton, J. A., Bouvier-Brown, N. C., Goldstein, A. H., Park, J. H., McKay, M., Matross, D. M., Mao, J., Brune, W. H., LaFranchi, B. W., Browne, E. C., Min, K. E., Wooldridge, P. J., Cohen, R. C., Crounse, J. D., Faloona, I. C., Gilman, J. B., Kuster, W. C., de Gouw, J. A., Huisman, A., and Keutsch, F. N.: The Chemistry of Atmosphere-Forest Exchange (CAFE) Model - Part 2: Application to BEARPEX-2007 observations, Atmos Chem Phys, 11, 1269-1294, 10.5194/acp-11-1269-2011, 2011.

Xu, D., Ge, B., Wang, Z., Sun, Y., Chen, Y., Ji, D., Yang, T., Ma, Z., Cheng, N., Hao, J., and Yao, X.: Below-cloud wet scavenging of soluble inorganic ions by rain in Beijing during the summer of 2014, Environ Pollut, 230, 963-973, https://doi.org/10.1016/j.envpol.2017.07.033, 2017.

Xu, D., Ge, B., Chen, X., Sun, Y., Cheng, N., Li, M., Pan, X., Ma, Z., Pan, Y., and Wang, Z.: Multimethod determination of the below-cloud wet scavenging coefficients of aerosols in Beijing, China, Atmos. Chem. Phys. Discuss., 2019, 1-26, 10.5194/acp-2019-680, 2019.

Xu, W., Luo, X. S., Pan, Y. P., Zhang, L., Tang, A. H., Shen, J. L., Zhang, Y., Li, K. H., Wu, Q. H., Yang, D. W., Zhang, Y. Y., Xue, J., Li, W. Q., Li, Q. Q., Tang, L., Lu, S. H., Liang, T., Tong, Y. A., Liu, P., Zhang, Q., Xiong, Z. Q., Shi, X. J., Wu, L. H., Shi, W. Q., Tian, K., Zhong, X. H., Shi, K., Tang, Q. Y., Zhang, L. J., Huang, J. L., He, C. E., Kuang, F. H., Zhu, B., Liu, H., Jin, X., Xin, Y. J., Shi, X. K., Du, E. Z., Dore, A. J., Tang, S., Collett, J. L., Goulding, K., Sun, Y. X., Ren, J., Zhang, F. S., and Liu, X. J.: Quantifying atmospheric nitrogen deposition through a nationwide monitoring network across China, Atmos Chem Phys, 15, 12345-12360, 2015.

Yamartino, R. J.: Nonnegative, conserved scalar transport using grid-cell-centered, spectrally constrained Blackman cubics for applications on a variable-thickness mesh, Mon. Weather Rev., 121, 753–763, 1993.

Yuan, J., Ling, Z., Wang, Z., Lu, X., Fan, S., He, Z., Guo, H., Wang, X., and Wang, N.: PAN-Precursor Relationship and Process Analysis of PAN Variations in the Pearl River Delta Region, Atmosphere-Basel, 9, 10.3390/atmos9100372, 2018.

Zaveri, R. A., and Peters, L. K.: A new lumped structure photochemical mechanism for large-scale applications, J. Geophys. Res., 104, 30387–30415, 1999.

Zhang, L., Brook, J. R., and Vet, R.: A revised parameterization for gaseous dry deposition in air-quality models, Atmos.chem.phys, 3, 2067-2082, 2003.

Zhao, Y., Duan, L., Xing, J., Larssen, T., Nielsen, C. P., and Hao, J. M.: Soil Acidification in China: Is Controlling SO2 Emissions Enough?, Environ Sci Technol, 43, 8021-8026, 2009.

Tables

Table 1. Mechanism and parameterization of deposition part of MICS-Asia III

No	M1	M2	M4	M5	M6	M11	M12	M13	M14
Model-(version)[a]	CMAQ v5.0.2	CMAQ v5.0.2	CMAQ v4.7.1	CMAQ v4.7.1	CMAQ v4.7.1	NAQPMS	NHM-Chem	GEOS-Chem	CMAQ v4.7.1
Advection-H[b]	Yamo	Yamo	PPM	PPM	Yamo	WA	WA	TPCORE	PPM
Advection-V[b]	PPM	PPM	PPM	PPM	Yamo	WA	WA	TPCORE	PPM
Diffusion-H[b]	multiscale	multiscale	multiscale	multiscale	multiscale	BD	multiscale	HB	multiscale
Diffusion-V[b]	ACM2	ACM2	ACM2	ACM2	ACM2	K-theory	MYJ	HB	ACM2
Gas-Chemistry[c]	SAPRC-99	SAPRC-99	SAPRC-99	SAPRC-99	SAPRC-99	CBMZ	SAPRC-99	Bey	SAPRC-99
Aerosol-chemistry[d]	AERO6 ISORROPIA (v2.1)	AERO6 ISORROPIA (v2.1)	AERO5 ISORROPIA (v1.7)	AERO5 ISORROPIA (v1.7)	AERO5 ISORROPIA (v1.7)	ISORROPIA (v1.7)	ISORROPIA (v2.1)	ISORROPIA (2.1)	ISORROPIA (v1.7)
Cloud & Aqueous[e]	ACM-AE6	ACM-AE6	ACM-AE5	ACM_AE5	ACM_AE5	Ge	WC	Jacob	ACM
Dry dep[f]	M3DRY	M3DRY	M3DRY	M3DRY	M3DRY	Wesely	Kajino	Wesely & Wang	M3DRY
Wet dep[g]	Foley	Foley	Foley	Foley	ACM	Ge	Kajino	Liu	Foley
Met	WRF	WRF	WRF	WRF	WRF	WRF	WRF	GEOS-5	RAMS
Emission[h]	standard	standard	standard	standard	standard	standard	standard	standard	standard

[a]: References for the advection scheme are as follows: Yamo:Yamartino, 1993; PPM: Piecewise Parabolic Method (Colella and Woodward, 1984); WA: Walcek and Aleksic, 1998; TPCORE: Wang et al., 2004.

[b]: References for diffusion scheme are as follows: ACM2: Asymmetric Convective Model version 2 (Pleim, 2007a,b); BD: Byun and Dennis, 1995; HB: Holtslag and Boville, 1993; multiscale: Byun and Schere, 2006; MYJ: Janjic, 1994.

[c]: References for the gas phase chemistry are as follows: Bey: Bey et al., 2001; CBMZ: Zaveri and Peters, 1999; SAPRC-99: Carter, 2000.

[d]: References for the aerosol chemistry are as follows: ISORROPIA version 2.1: Fountoukis and Nenes, 2007; version 1.7: Nenes et al., 1998.

[e]: References for the Cloud & Aqueous are as follows: Ge: Ge et al., 2014; WC: Walcek,1986 and Carlton, 2007; Jacob: Jacob, 2000;

[f]: References for the dry deposition scheme are as follows: M3DRY: Pleim et al., 2001; Kajino: Kajino et al., 2018; Wang: Wang et al., 2004; Wesely: Wesely, 1989.

[g]: References for the wet deposition scheme are as follows: Foley: Foley et al, 2010; Ge: Ge et al., 2014; Kajino: Kajino et al., 2018; Liu: Liu et al., 2001.

[h]: "standard" indicates the basic emission inventories in Phase III.

1108 Table 2. Statistical parameters of oxidized N deposition for urban, rural and whole China.

Urban (N=49)	OBS	M1	M2	M4	M5	M6	M11	M12	M13	M14
	Oxidized N deposition (kg N ha^{-1})									
R		0.24	0.25	0.28	0.27	0.26	0.25	0.40	0.37	0.22
NMB%		16.8%	-44.5%	-19.3%	38.5%	-15.8%	48.2%	-5.3%	-7.2%	-52.7%
NME%		56.4%	60.4%	51.3%	64.0%	51.0%	67.1%	46.9%	44.2%	59.1%
FAC2%		63.3%	32.7%	51.0%	57.1%	57.1%	59.2%	57.1%	61.2%	40.8%
Mean	7.1	8.3	3.9	5.7	9.9	6.0	10.5	6.7	6.6	3.4
	Oxidized N concentration in rainfall (mg N/L)									
R		0.60	0.57	0.60	0.62	0.59	0.49	0.61	0.52	0.50
NMB%		26.8%	-37.9%	-11.3%	49.3%	-6.7%	75.9%	2.7%	19.3%	-31.3%
NME%		57.6%	51.4%	46.0%	69.0%	47.5%	94.8%	47.4%	65.5%	60.0%
FAC2%		59.2%	42.9%	59.2%	51.0%	59.2%	51.0%	61.2%	49.0%	34.7%
Mean	0.9	1.1	0.5	0.8	1.3	0.8	1.5	0.9	1.0	0.6
Rural (N=34)	Oxidized N deposition (kg N ha^{-1})									
R		0.09	0.05	0.09	0.14	0.09	0.28	0.26	0.23	0.30
NMB%		55.4%	-27.8%	5.1%	86.9%	9.9%	102.5%	11.5%	13.6%	-37.6%
NME%		83.7%	57.8%	59.9%	103.3%	60.5%	110.1%	54.4%	56.0%	50.3%
FAC2%		55.9%	41.2%	50.0%	35.3%	47.1%	38.2%	55.9%	55.9%	50.0%
Mean	5.4	8.5	3.9	5.7	10.2	6.0	11.0	6.1	6.2	3.4
	Oxidized N concentration in rainfall (mg N/L)									
R		0.43	0.41	0.44	0.46	0.44	0.48	0.47	0.35	0.43
NMB%		20.5%	-43.0%	-17.1%	45.2%	-13.4%	63.2%	-9.4%	-0.2%	-43.2%
NME%		65.4%	55.6%	54.2%	76.3%	53.8%	89.2%	53.8%	62.7%	53.3%
FAC2%		44.1%	38.2%	41.2%	41.2%	44.1%	41.2%	47.1%	32.4%	41.2%

Mean	0.9	1.0	0.5	0.7	1.2	0.7	1.4	0.8	0.9	0.5
All sites (N=83)					Oxidized N deposition (kg N ha^{-1})					
R		0.2	0.17	0.21	0.21	0.19	0.24	0.37	0.33	0.23
NMB%		30.3%	-38.7%	-10.7%	55.4%	-6.8%	67.2%	0.6%	0.1%	-47.4%
NME%		66.0%	59.5%	54.3%	77.8%	54.3%	82.2%	49.5%	48.3%	56.0%
FAC2%		60.2%	36.1%	50.6%	48.2%	53.0%	50.6%	56.6%	59.0%	44.6%
Mean	6.4	8.4	3.9	5.7	10.0	6.0	10.7	6.5	6.4	3.4
					Oxidized N concentration in rainfall (mg N/L)					
R		0.53	0.51	0.54	0.56	0.53	0.48	0.56	0.46	0.46
NMB%		24.2%	-40.0%	-13.7%	47.6%	-9.5%	70.7%	-2.3%	11.3%	-36.2%
NME%		60.8%	53.1%	49.4%	72.0%	50.1%	92.5%	50.0%	64.4%	57.3%
FAC2%		53.0%	41.0%	51.8%	47.0%	53.0%	47.0%	55.4%	42.2%	37.3%
Mean	0.9	1.1	0.5	0.7	1.3	0.8	1.5	0.8	1.0	0.5

1111 Table 3. Same as Table 2 but for reduced N deposition.

Urban (N=49)	OBS	M1	M2	M4	M5	M6	M11	M12	M13	M14
	Reduced N deposition (kg N ha^{-1})									
R		0.30	0.31	0.33	0.34	0.32	0.41	0.33	0.49	0.05
NMB%		-38.2%	-43.0%	-45.6%	-43.9%	-37.3%	-73.5%	-38.8%	-38.8%	-60.2%
NME%		50.7%	52.2%	52.9%	51.4%	49.8%	73.5%	50.0%	46.3%	64.1%
FAC2%		53.1%	44.9%	42.9%	46.9%	51.0%	16.3%	51.0%	55.1%	34.7%
Mean	10.9	6.7	6.2	5.9	6.1	6.8	2.9	6.7	6.7	4.3
	Reduced N concentration in rainfall (mg N/L)									
R		0.83	0.83	0.84	0.84	0.83	0.77	0.86	0.75	0.56
NMB%		-38.0%	-42.6%	-42.2%	-40.6%	-36.1%	-73.8%	-41.1%	-22.1%	-48.8%
NME%		44.5%	47.5%	47.4%	46.0%	43.7%	73.8%	43.7%	46.0%	62.1%
FAC2%		57.1%	51.0%	42.9%	51.0%	55.1%	10.2%	57.1%	44.9%	24.5%
Mean	1.5	0.9	0.9	0.9	0.9	1.0	0.4	0.9	1.2	0.8
Rural (N=34)	Reduced N deposition (kg N ha^{-1})									
R		0.29	0.29	0.28	0.30	0.32	0.27	0.28	0.52	0.44
NMB%		-14.4%	-22.0%	-21.1%	-18.3%	-13.6%	-62.5%	-23.2%	-19.0%	-46.2%
NME%		48.0%	47.7%	48.1%	46.5%	47.2%	68.5%	45.8%	40.8%	49.4%
FAC2%		70.6%	55.9%	58.8%	61.8%	67.6%	23.5%	61.8%	73.5%	52.9%
Mean	9.0	7.7	7.0	7.1	7.3	7.7	3.4	6.9	7.3	4.8
	Reduced N concentration in rainfall (mg N/L)									
R		0.79	0.79	0.81	0.82	0.80	0.74	0.82	0.69	0.55
NMB%		-27.5%	-34.2%	-31.9%	-29.7%	-26.4%	-69.0%	-33.8%	-20.2%	-47.4%
NME%		37.7%	40.6%	39.0%	36.6%	37.1%	69.6%	37.9%	40.5%	56.9%
FAC2%		52.9%	52.9%	52.9%	52.9%	55.9%	17.6%	52.9%	64.7%	44.1%

Mean	1.3	1.0	0.9	0.9	0.9	1.0	0.4	0.9	1.1	0.7
All sites (N=83)					Reduced N deposition (kg N ha^{-1})					
R		0.26	0.27	0.26	0.27	0.28	0.30	0.29	0.48	0.20
NMB%		-29.6%	-35.3%	-36.7%	-34.5%	-28.6%	-69.5%	-33.1%	-31.6%	-55.1%
NME%		49.7%	50.6%	51.2%	49.6%	48.9%	71.7%	48.5%	44.3%	58.7%
FAC2%		60.2%	49.4%	49.4%	53.0%	57.8%	19.3%	55.4%	62.7%	42.2%
Mean	10.1	7.1	6.5	6.4	6.6	7.2	3.1	6.8	6.9	4.5
					Reduced N concentration in rainfall (mg N/L)					
R		0.81	0.81	0.82	0.83	0.81	0.75	0.84	0.73	0.56
NMB%		-34.0%	-39.4%	-38.2%	-36.4%	-32.3%	-71.9%	-38.3%	-21.3%	-48.3%
NME%		41.9%	44.9%	44.2%	42.3%	41.2%	72.2%	41.5%	43.9%	60.1%
FAC2%		55.4%	51.8%	47.0%	51.8%	55.4%	13.3%	55.4%	53.0%	32.5%
Mean	1.4	0.9	0.9	0.9	0.9	1.0	0.4	0.9	1.1	0.7

1112

1113 Table 4. Types of depositions and its relevant contributions to TIN as well as the
1114 emissions of reduced and oxidized N in different regions (Unit: kg N/ha/yr).

Regions		NC	NE	NW	SE	SW	TP	China
Types of deposition	gHNO3d	4.9	1.8	0.8	5.8	2.4	0.2	2.1
	gNH3d	6.7	1.8	0.5	3.7	3.0	0.5	2.0
	gNOxd	1.2	0.3	0.1	1.0	0.3	0.0	0.3
	pNH4d	1.9	0.5	0.2	1.5	0.8	0.1	0.6
	pNO3d	1.3	0.4	0.1	1.2	0.4	0.0	0.4
	pNH4w	7.0	2.6	0.8	7.0	5.2	1.3	3.2
	pNO3w	6.3	2.7	0.7	6.9	3.0	0.6	2.6
	N_{rd}	15.6	4.9	1.6	12.2	9.0	1.9	5.9
	N_{ox}	13.6	5.2	1.6	14.9	6.0	0.8	5.4
	Wet TIN	13.3	5.3	1.5	13.9	8.2	1.9	5.8
	Dry TIN	16.0	4.8	1.7	13.2	6.9	0.8	5.5
	TIN	29.2	10.1	3.1	27.0	15.0	2.7	11.3
N_{rd}/TIN %	This study	53	49	52	45	60	70	52
	NNDMN							58
	HTAP							>60
Wet/TIN %	This study	46	52	48	51	55	70	51
	NNDMN	43	46	39	58	45	50	48
	HTAP	40~50	40~60	30~60	~60	60~70	60~70	
Emission	N_{rd}	24.4	4.9	2.9	21.6	13.1	0.7	8.7
	N_{ox}	30.4	5.6	3.1	21.4	6.4	0.2	8.3
	TIN	54.8	10.5	5.9	43.0	19.5	0.9	17.1
Dep/Emi %	N_{rd}	64	100	55	56	69	271	67
	N_{ox}	45	93	52	70	94	400	65
	TIN	53	96	53	63	77	300	66
Critical load	SSMB1	10~30	5~20	<5	10~20	>20	10~15	
	Empirical*	>200	<15	<15	50~200	50~200	20~50	
	SSMB2	>50	14-50	<14	20-50	10~30	~14	

1115 1, Duan et al.,2, Zhao et al.,* Liu et al.,,

Figures and captions

Figure 1: Locations of the measurement sites and the distribution of the ID.

Figure 2: Percentile Box plot of oxidized N wet deposition simulated in each model and compared with the observation as well as the rainfalls, with 99% and 1% represented for the high and low points, 90% and 10% represented for the top and bottom horizontal lines, 75% and 25% represented for the upper and lower edge of the box and asterisk and long horizontal line in the middle of the box represented for the medium and mean value, respectively.

Figure 3: Monthly variation of simulated wet deposition of oxidized N compared with the observations in urban sites (a) and rural sites (b) of NC; urban sites (c) and rural sites (d) of NE; as well as of reduced N in urban sites (e) and rural sites (f) of NC; urban sites (g) and rural sites (h) of NE.

Figure 4: Same as Figure 2 but for reduced N wet depositions.

Figure 5: Distributions of the wet depositions of N_{ox} simulated by M1~M14 (a)~(i), ENM of the multi-models (j) MICS-Asia III, observation from multi-source measurements (k) and the comparison between ENM and observations (l) ($kgN \bullet ha^{-1}$).

Figure 6: Same as Figure 5 but for N_{rd}.

Figure 7: Spatial distribution of CV of (a) N_{ox} dry deposition, (b) N_{rd} dry deposition, (c) N_{ox} wet deposition and (d) N_{rd} wet deposition in MICS-Asia III on the annual and seasonal basis.

Figure 8: Distribution of CV of NO_x (a), NO_3^- (b), NH_3 (c) and NH_4^+ (d) in the air mass for seasonal and annual.

Figure 9: ENM results for dry deposition (a) and wet deposition (b) of N_{ox}, VCD of NO_2 from SCIAMACHY (c) and NO_x emission from MICS-Asia (d); ENM results for dry deposition (e) and wet deposition (f) of N_{rd}, VCD of NH_3 from IASI (g) and NH_3 emission from MICS-Asia (h).

Figure 10: ENM results of each process of N deposition flux (a) and the fraction in TIN (b) in MICS-Asia III. The icons w_N, w_A, d_NO2, d_NH3, d_HNO3, d_ammonium and d_nitrate represented wet deposition of nitrate, wet deposition of ammonium, dry deposition of NH_3, dry deposition of HNO_3, dry deposition of ammonium and dry deposition of nitrate, respectively.

Figure 11: Pathway of N species to TIN deposition in different regions from ENM results (a), and TIN depositions by wet or dry deposited manner (b) in percentile Box plot; with 90% and 10% represented for the top and bottom horizontal line, 75% and 25% represented for the upper and lower edge of the box and asterisk in the middle of

1151 the box represented for the medium value, respectively.

1152 **Figure 12:** Relationship of N_{rd} deposition vs. NH_3 emission (a) and relationship of

1153 N_{ox} deposition vs. NO_x emission (b) in each region of China.

1154

1155

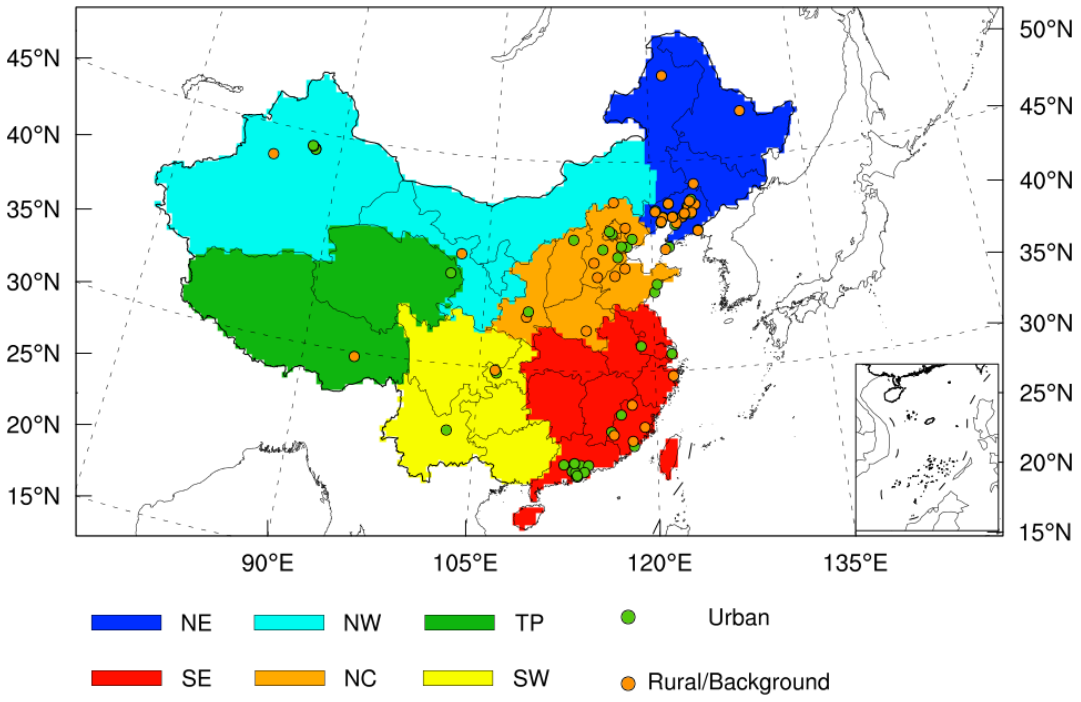

1156

1157 Figure 1: Locations of the measurement sites and the distribution of the ID.

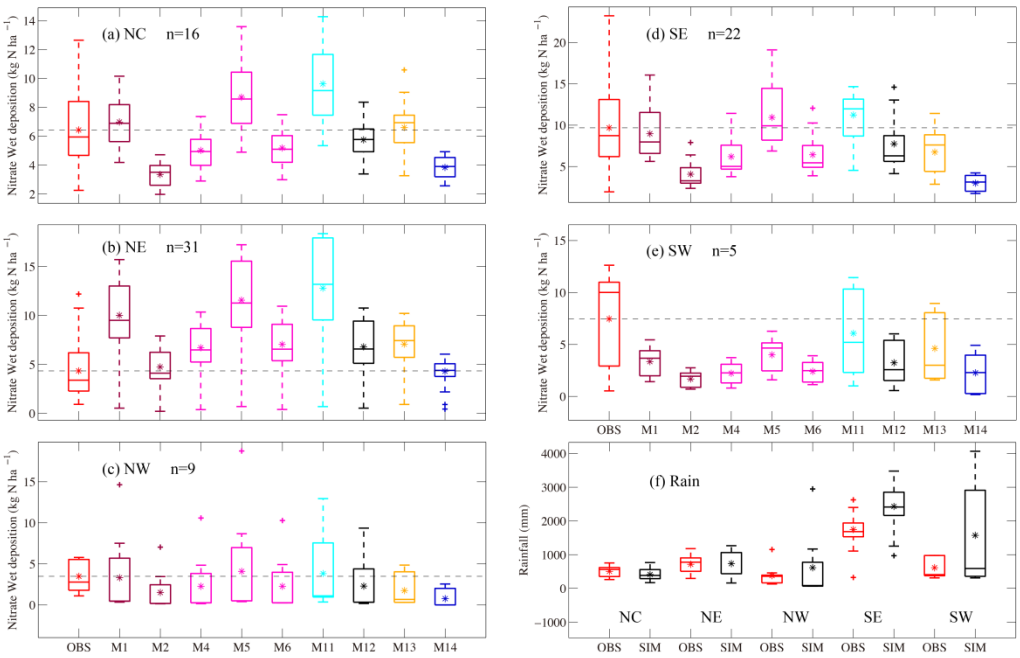

Figure 2: Percentile Box plot of oxidized N wet deposition simulated in each model and compared with the observation as well as the rainfalls, with 99% and 1% represented for the high and low points, 90% and 10% represented for the top and bottom horizontal lines, 75% and 25% represented for the upper and lower edge of the box and asterisk and long horizontal line in the middle of the box represented for the medium and mean value, respectively.

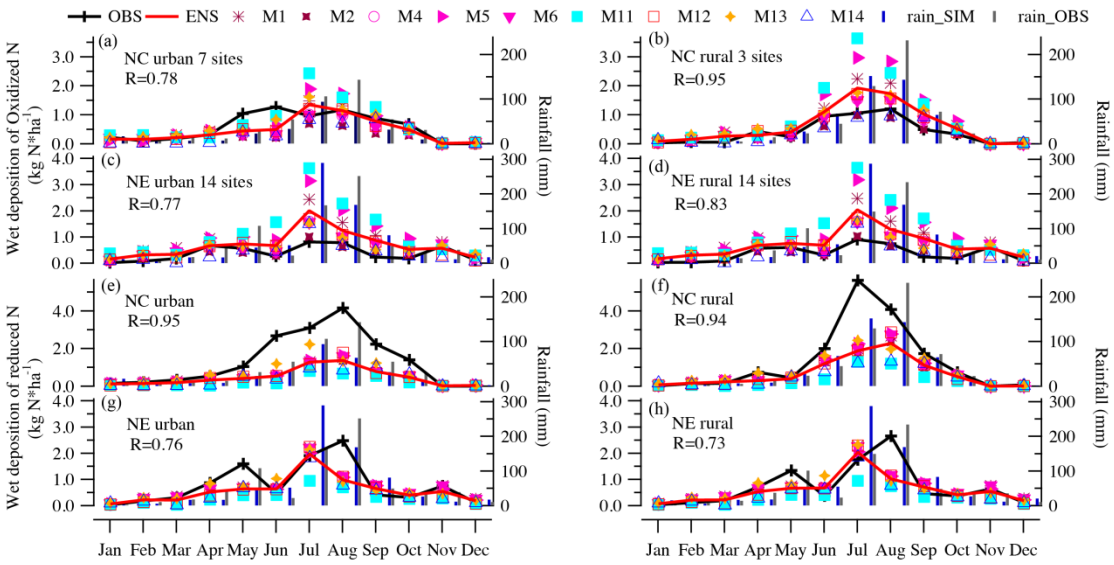

Figure 3: Monthly variation of simulated wet deposition of oxidized N compared with the observations in urban sites (a) and rural sites (b) of NC; urban sites (c) and rural sites (d) of NE; as well as of reduced N in urban sites (e) and rural sites (f) of NC; urban sites (g) and rural sites (h) of NE.

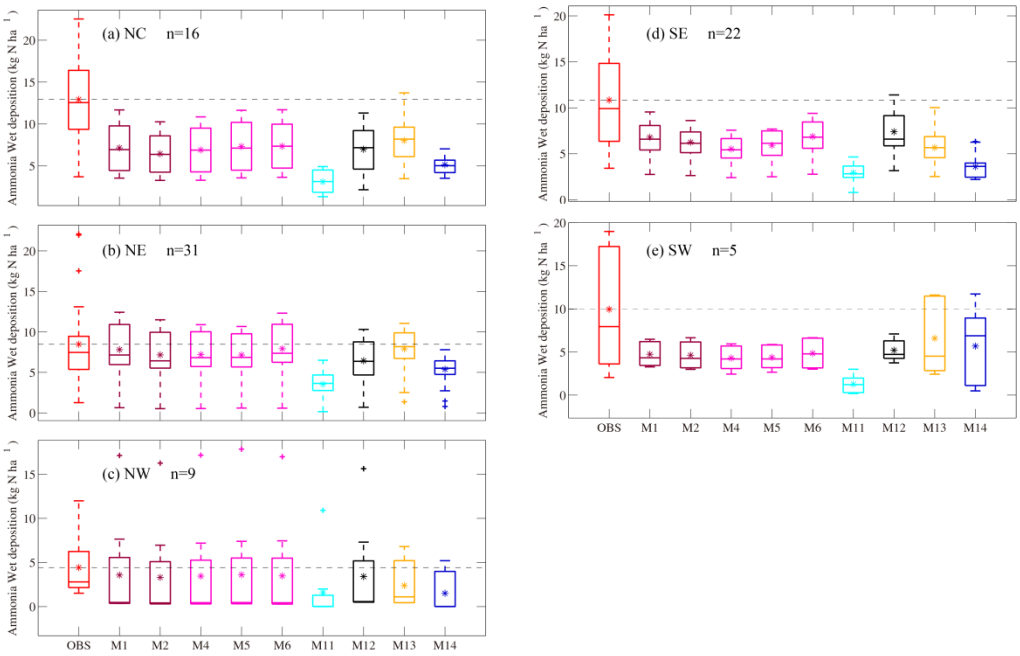

Figure 4: Same as Figure 2 but for reduced N wet depositions.

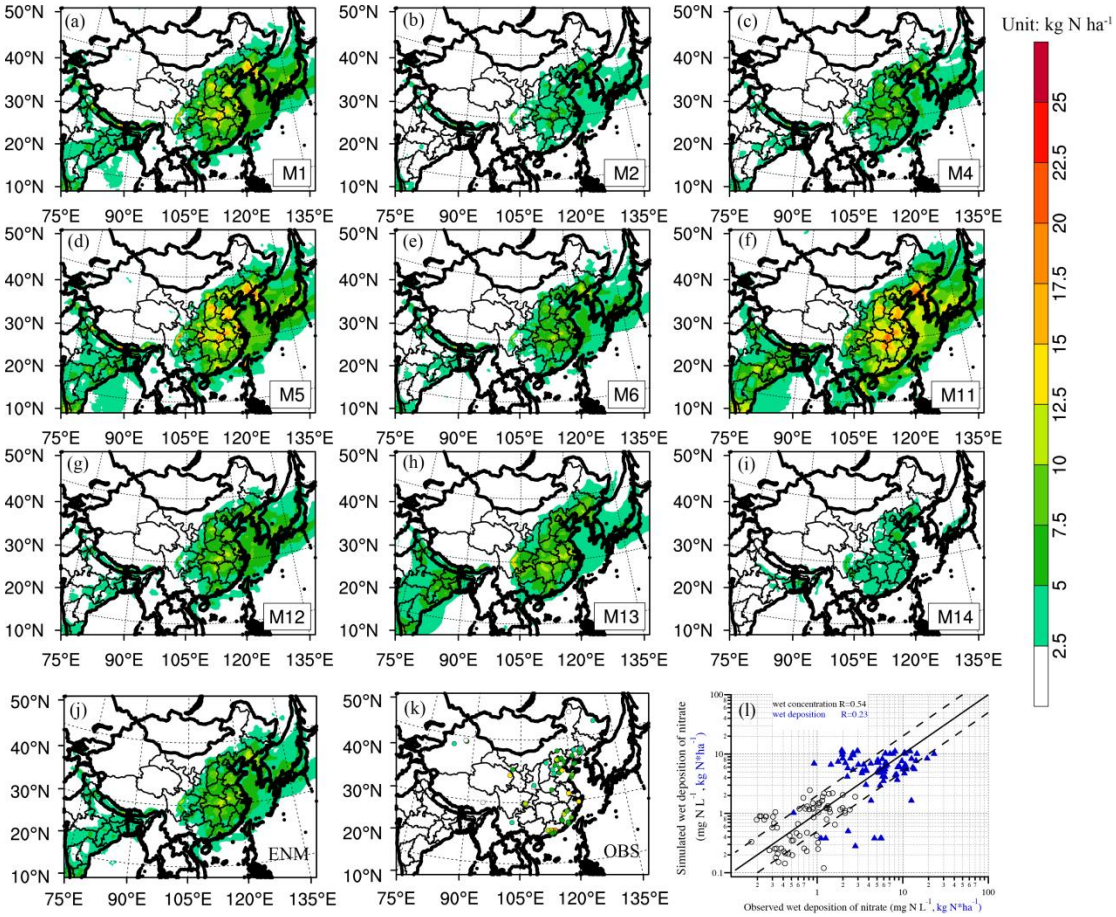

Figure 5: Distributions of the wet depositions of N_{ox} simulated by M1~M14 (a)~(i), ENM of the multi-models (j) MICS-Asia III, observation from multi-source measurements (k) and the comparison between ENM and observations (l) ($kgN \bullet ha^{-1}$).

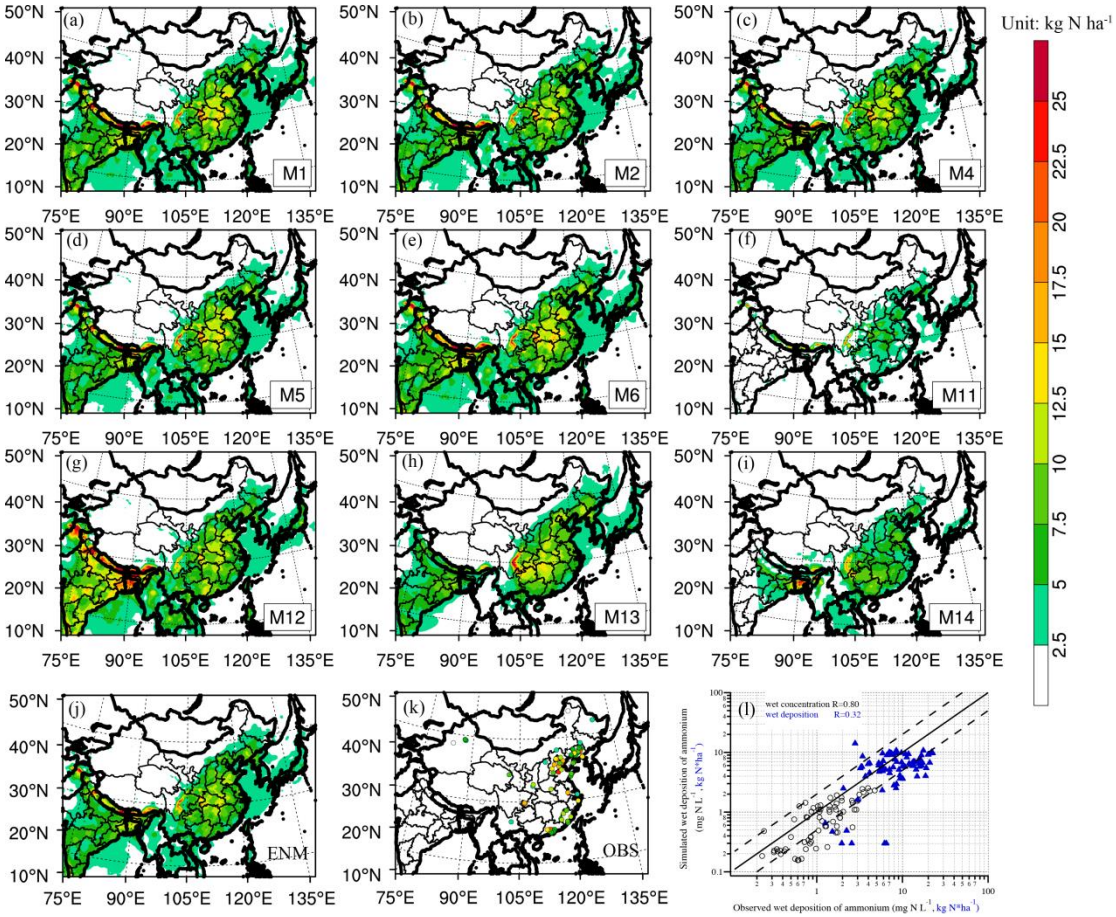

Figure 6: Same as Figure 5 but for $N_{rd.}$

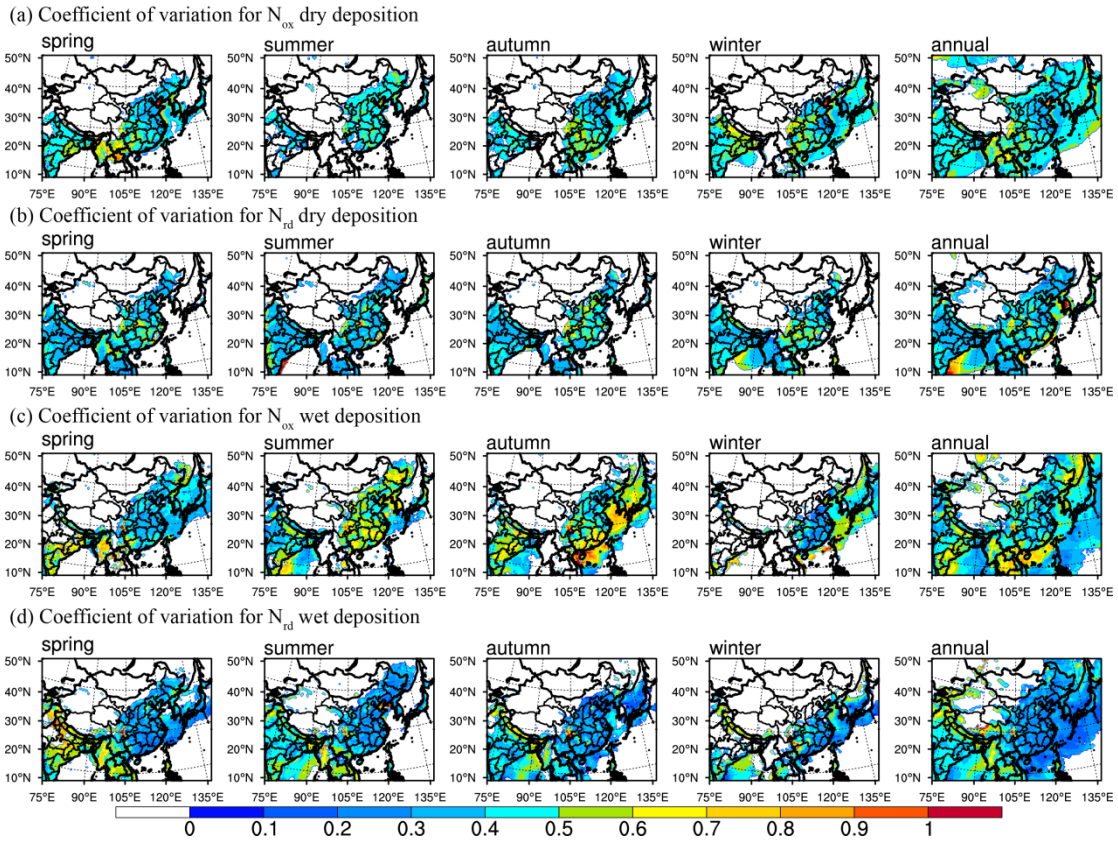

Figure 7: Spatial distribution of CV of (a) N_{ox} dry deposition, (b) N_{rd} dry deposition, (c) N_{ox} wet deposition and (d) N_{rd} wet deposition in MICS-Asia III on the annual and seasonal basis.

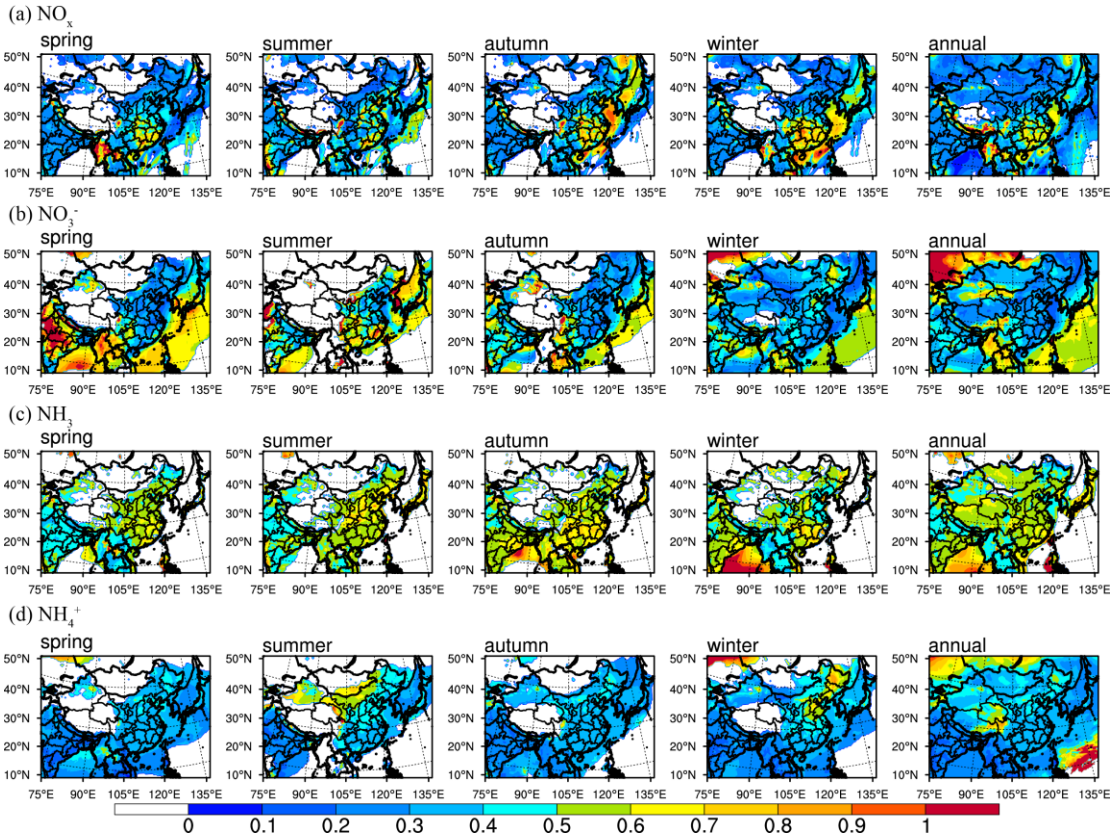

Figure 8: Distribution of CV of NO_x (a), NO_3^- (b), NH_3 (c) and NH_4^+ (d) in the air mass for seasonal and annual.

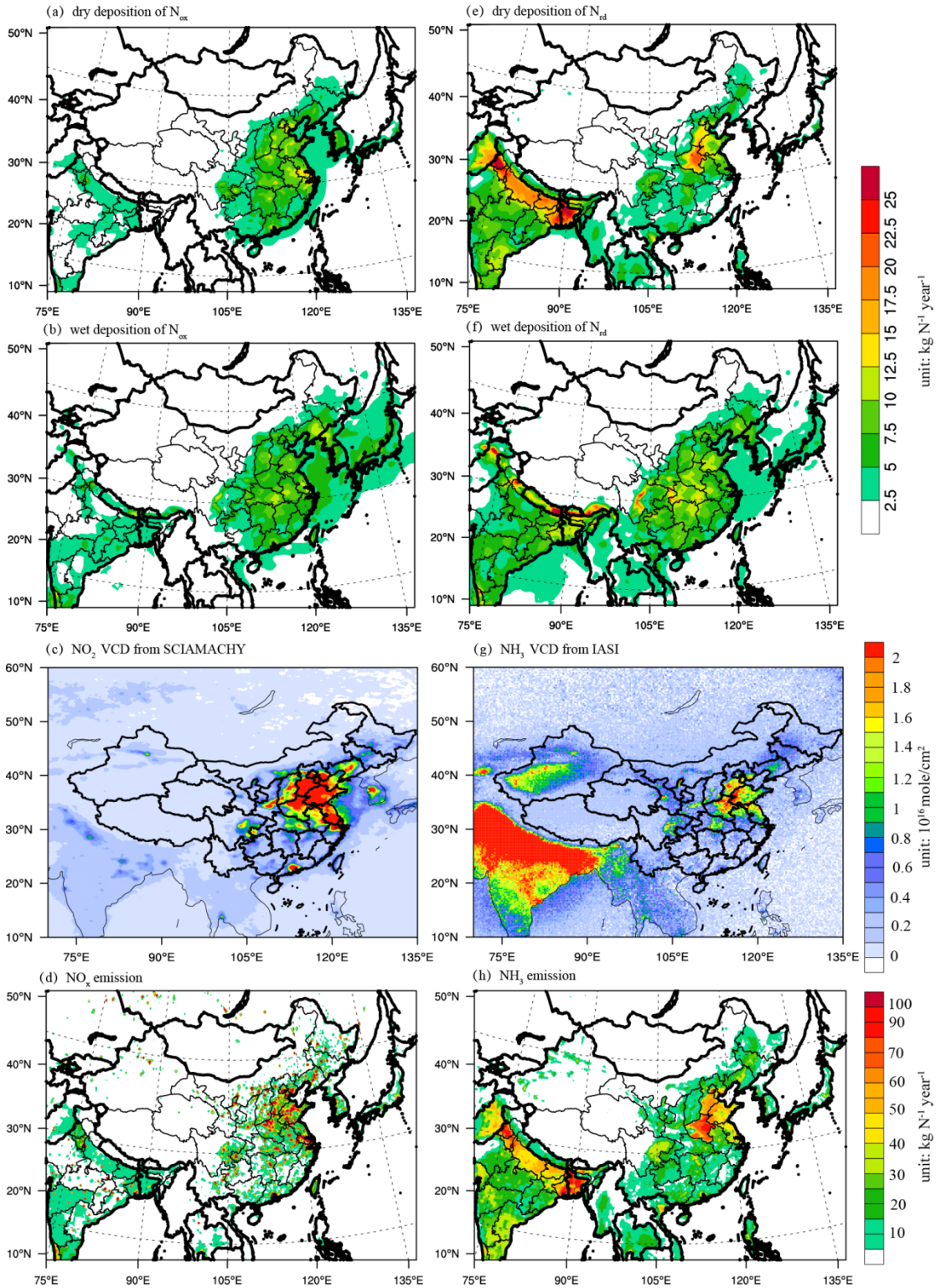

Figure 9: ENM results for dry deposition (a) and wet deposition (b) of N_{ox}, VCD of NO_2 from SCIAMACHY (c) and NO_x emission from MICS-Asia (d); ENM results for dry deposition (e) and wet deposition (f) of N_{rd}, VCD of NH_3 from IASI (g) and NH_3 emission from MICS-Asia (h).

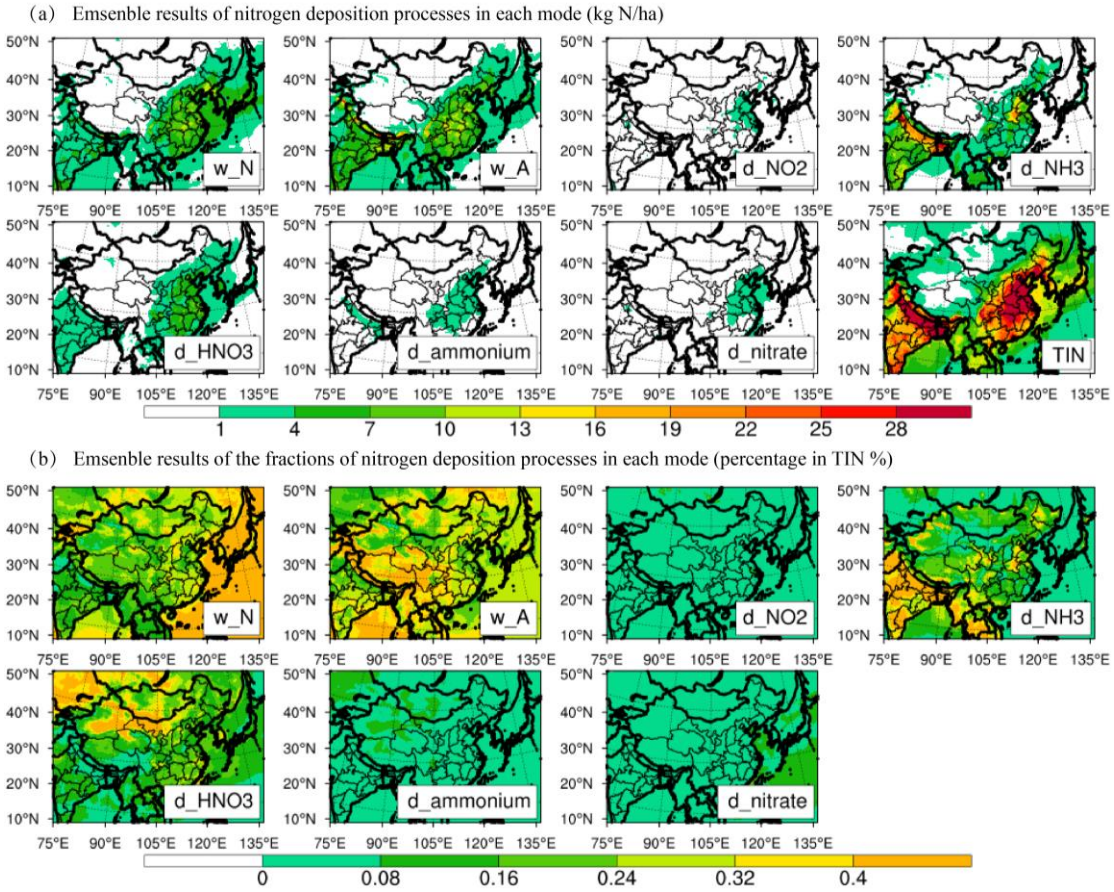

Figure 10: ENM results of each process of N deposition flux (a) and the fraction in TIN (b) in MICS-Asia III. The icons w_N, w_A, d_NO2, d_NH3, d_HNO3, d_ammonium and d_nitrate represent wet deposition of nitrate, wet deposition of ammonium, dry deposition of NH_3, dry deposition of HNO_3, dry deposition of ammonium and dry deposition of nitrate, respectively.

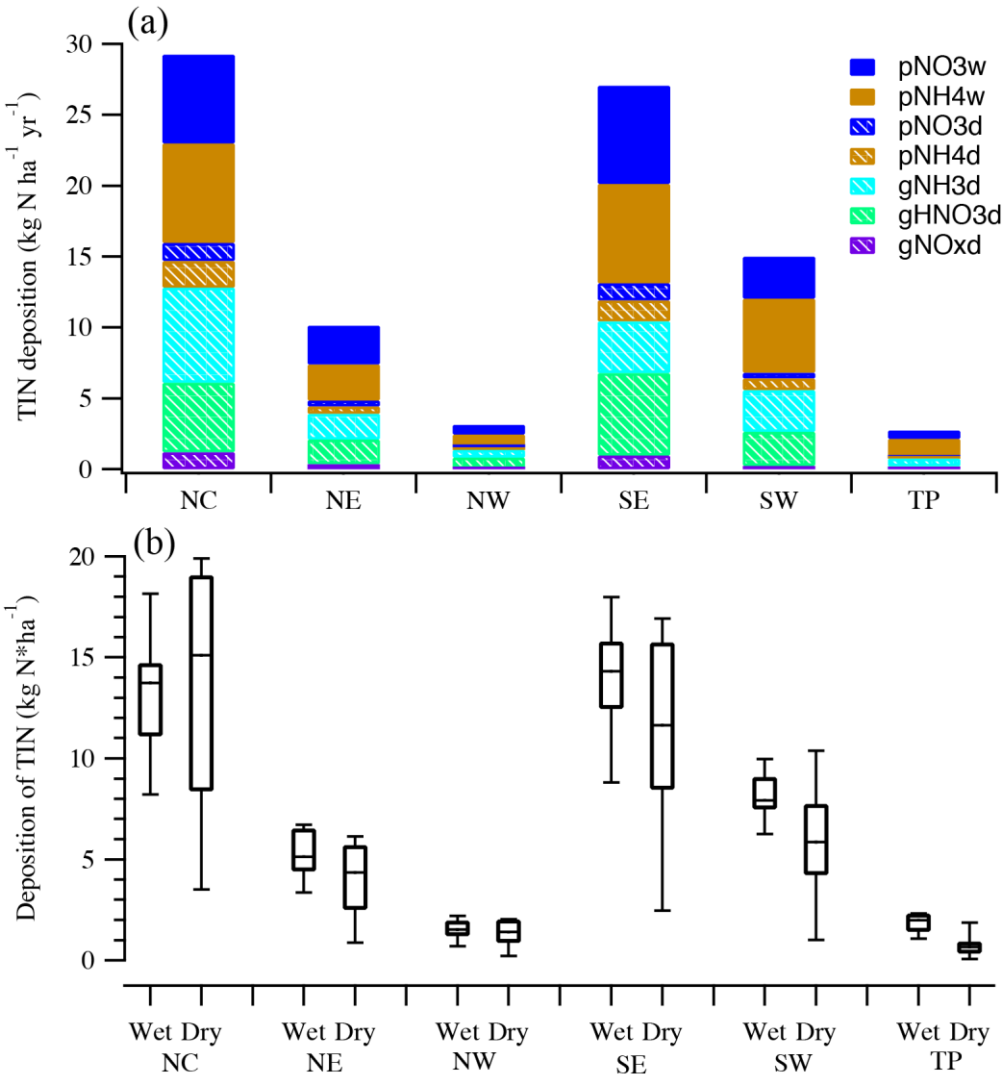

Figure 11: Pathway of N species to TIN deposition in different regions from ENM results (a), and TIN depositions by wet or dry deposited manner (b) in percentile Box plot; with 90% and 10% represented for the top and bottom horizontal line, 75% and 25% represented for the upper and lower edge of the box and asterisk in the middle of the box represented for the medium value, respectively.

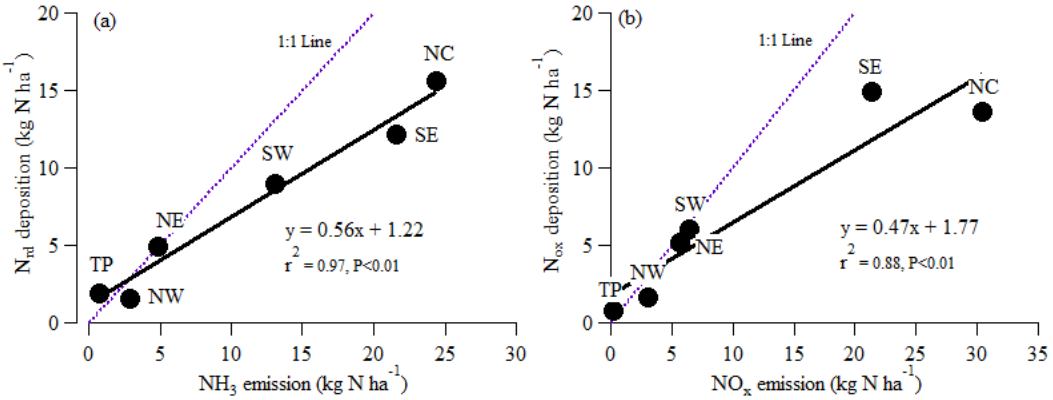

Figure 12: Relationship of N_{rd} deposition vs. NH_3 emission (a) and relationship of N_{ox} deposition vs. NO_x emission (b) in each region of China.